



**UNIVERSIDAD DE INVESTIGACIÓN DE TECNOLOGÍA
EXPERIMENTAL YACHAY**

Escuela de Ciencias Físicas y Nanotecnología

TÍTULO: Digital Compasses Calibration in KM3NeT

Trabajo de integración curricular presentado como requisito para la
obtención del título de Físico

Autor:

Bryan Daniel Darquea Chauca

Tutor:

Ph.D. - Yepes Ramírez Harold

Urcuquí, Julio 2021

SECRETARÍA GENERAL
(Vicerrectorado Académico/Cancillería)
ESCUELA DE CIENCIAS FÍSICAS Y NANOTECNOLOGÍA
CARRERA DE FÍSICA
ACTA DE DEFENSA No. UITEY-PHY-2021-00017-AD

A los 2 días del mes de julio de 2021, a las 16:00 horas, de manera virtual mediante videoconferencia, y ante el Tribunal Calificador, integrado por los docentes:

Presidente Tribunal de Defensa	Dr. BRAMER ESCAMILLA , WERNER , Ph.D.
Miembro No Tutor	Dr. GUEVARA GRANIZO, MARCO VINICIO , Ph.D.
Tutor	Dr. YEPES RAMIREZ, HAROLD , Ph.D.

El(la) señor(ita) estudiante **DARQUEA CHAUCA, BRYAN DANIEL**, con cédula de identidad No. **1804917472**, de la **ESCUELA DE CIENCIAS FÍSICAS Y NANOTECNOLOGÍA**, de la Carrera de **FÍSICA**, aprobada por el Consejo de Educación Superior (CES), mediante Resolución **RPC-SO-39-No.456-2014**, realiza a través de videoconferencia, la sustentación de su trabajo de titulación denominado: **Digital Compasses Calibration in KM3NeT** , previa a la obtención del título de **FÍSICO/A**.

El citado trabajo de titulación, fue debidamente aprobado por el(los) docente(s):

Tutor	Dr. YEPES RAMIREZ, HAROLD , Ph.D.
--------------	-----------------------------------

Y recibió las observaciones de los otros miembros del Tribunal Calificador, las mismas que han sido incorporadas por el(la) estudiante.

Previamente cumplidos los requisitos legales y reglamentarios, el trabajo de titulación fue sustentado por el(la) estudiante y examinado por los miembros del Tribunal Calificador. Escuchada la sustentación del trabajo de titulación a través de videoconferencia, que integró la exposición de el(la) estudiante sobre el contenido de la misma y las preguntas formuladas por los miembros del Tribunal, se califica la sustentación del trabajo de titulación con las siguientes calificaciones:

Tipo	Docente	Calificación
Tutor	Dr. YEPES RAMIREZ, HAROLD , Ph.D.	10,0
Presidente Tribunal De Defensa	Dr. BRAMER ESCAMILLA , WERNER , Ph.D.	10,0
Miembro Tribunal De Defensa	Dr. GUEVARA GRANIZO, MARCO VINICIO , Ph.D.	9,9

Lo que da un promedio de: **10 (Diez punto Cero)**, sobre 10 (diez), equivalente a: **APROBADO**

Para constancia de lo actuado, firman los miembros del Tribunal Calificador, el/la estudiante y el/la secretario ad-hoc.

Certifico que en cumplimiento del Decreto Ejecutivo 1017 de 16 de marzo de 2020, la defensa de trabajo de titulación (o examen de grado modalidad teórico práctica) se realizó vía virtual, por lo que las firmas de los miembros del Tribunal de Defensa de Grado, constan en forma digital.

DARQUEA CHAUCA, BRYAN DANIEL
Estudiante

Dr. BRAMER ESCAMILLA , WERNER , Ph.D.
Presidente Tribunal de Defensa

**WERNER
BRAMER
ESCAMILLA**
 Digitally signed by
 WERNER BRAMER
 ESCAMILLA
 Date: 2021.07.02
 17:11:50 -05'00'

Dr. YEPES RAMIREZ, HAROLD , Ph.D.
Tutor

**HAROLD YEPES
RAMIREZ**
 Firmado digitalmente por
 HAROLD YEPES RAMIREZ
 Fecha: 2021.07.02
 17:21:00 -05'00'

MARCO
VINICIO
GUEVARA
GRANIZO


Firmado digitalmente
por MARCO VINICIO
GUEVARA GRANIZO
Fecha: 2021.07.02
17:13:46 -05'00'

Dr. GUEVARA GRANIZO, MARCO VINICIO , Ph.D.
Miembro No Tutor

CIFUENTES TAFUR, EVELYN CAROLINA
Secretario Ad-hoc

EVELYN
CAROLINA
CIFUENTES
TAFUR

Digitally signed by
EVELYN CAROLINA
CIFUENTES TAFUR
Date: 2021.07.02
17:10:41 -05'00'



AUTORÍA

Yo, **BRYAN DANIEL DARQUEA CHAUCA**, con cédula de identidad 1804917472, declaro que las ideas, juicios, valoraciones, interpretaciones, consultas bibliográficas, definiciones y conceptualizaciones expuestas en el presente trabajo; así como, los procedimientos y herramientas utilizadas en la investigación, son de absoluta responsabilidad de el/la autora (a) del trabajo de integración curricular. Así mismo, me acojo a los reglamentos internos de la Universidad de Investigación de Tecnología Experimental Yachay.

Urcuquí, julio 2021.



Bryan Daniel Darquea Chauca
CI: 1804917472

AUTORIZACIÓN DE PUBLICACIÓN

Yo, **BRYAN DANIEL DARQUEA CHAUCA**, con cédula de identidad 1804917472, cedo a la Universidad de Tecnología Experimental Yachay, los derechos de publicación de la presente obra, sin que deba haber un reconocimiento económico por este concepto. Declaro además que el texto del presente trabajo de titulación no podrá ser cedido a ninguna empresa editorial para su publicación u otros fines, sin contar previamente con la autorización escrita de la Universidad.

Asimismo, autorizo a la Universidad que realice la digitalización y publicación de este trabajo de integración curricular en el repositorio virtual, de conformidad a lo dispuesto en el Art. 144 de la Ley Orgánica de Educación Superior

Urcuquí, julio 2021.



Bryan Daniel Darquea Chauca
CI: 1804917472

Dedicatoria

A mis padres Luis y Carmen, a mi hermana Madeleine y a mi mascota Max que alumbran mi camino con su amor.

Ab imo pectore

Bryan Daniel Darquea Chauca

Acknowledgments

I want to especially thank Dorothea, Robert, Giorgio, Miquel, Juan, Chiara, and Didac for their valuable contribution to the development of this work. In the same way, to all the members of the KM3NeT Collaboration for allowing me to work with them and significantly learn the value of teamwork and greatly increase my experience as a researcher.

Additionally, I am very grateful to all the Faculty of Physical Sciences and Nanotechnology professors for sharing their knowledge with me throughout my time at the university. I especially appreciate the support of my tutor Harold Yepes Ramírez, for sharing his friendship, knowledge, and experience that has allowed me to develop this work.

I would particularly like to thank my parents Luis and Carmen, and my sister Madeleine for being part of my life and giving me their full support throughout my career. I especially want to thank Sol for her support to reach my goals. In addition, I want to thank my friends Francisco, Lenin, Rony, Joshua, and Pol. Thanks to all of you for the memories that I will always remember.

Bryan Daniel Darquea Chauca

Resumen

La Colaboración KM3NeT es el equipo mas grande de científicos e ingenieros operando la mas grande infraestructura de investigación multipropósito, multidisciplinar submarina en el fondo del Mar Mediterráneo, incorporando una red de telescopios de neutrinos de nueva generación y dispositivos dedicados a ciencias multidisciplinarias. KM3NeT está actualmente escalando dos detectores de neutrinos de gran volumen ($\sim\text{km}^3$), compartiendo la misma tecnología pero con diferentes diseños y objetivos científicos. Estos detectores son los llamados ORCA (investigación de oscilación con cósmicos en el abismo) y ARCA (investigación de astropartículas con cósmicos en el abismo). ARCA se encuentra en el sitio KM3NeT-It (Capo Passero, Italia) y ORCA está en el sitio KM3NeT-Fr (Toulon, Francia). El principio de detección se basa en el registro de la luz de Cherenkov, inducida por partículas cargadas relativistas producidas en interacciones de neutrinos al cruzar los detectores. Cada detector comprende una matriz tridimensional (3D) de unidades de detección (DU), en un diseño modular. Cada DU comprende 18 módulos ópticos digitales (DOMs), y cada DOM contiene 31 tubos fotomultiplicadores (PMT) de 3 pulgadas, responsables de registrar la luz Cherenkov. Cada DOM recopila información que permite la reconstrucción de la dirección, energía y tiempo relacionado a eventos de neutrinos. Los detectores funcionan en el modo all-data-to-shore de transferencia de datos para el análisis posterior de esta información.

Conocer la orientación de cada DOM es crucial para determinar la direccionalidad de los eventos de interés en KM3NeT. Dentro de cada DOM específicamente en la llamada CLB, se integra una brújula digital compuesta por un acelerómetro 3D y un magnetómetro 3D, a cargo de la lectura de inclinación y orientación (*Yaw, Pitch y Roll*). En el presente trabajo, se definió un procedimiento de calibración para el subsistema de posicionamiento de la brújula, identificando los parámetros de calibración necesarios para mitigar las incertidumbres vinculadas al dispositivo. Además, se realiza un estudio crudo acerca de la estimación de incertidumbres para el subsistema de posicionamiento de brújulas de KM3NeT y se propone una parametrización preliminar. Como resultado, se verifica que se cumple la orientación requerida para cumplir con los objetivos físicos de KM3NeT: la precisión de la orientación debe ser menor a 3.5° , esencial para garantizar la reconstrucción óptima de eventos tipo-neutrino a partir de la reconstrucción sus trayectorias. El análisis de datos en este trabajo apunta a una precisión de orientación mejorada.

Palabras clave: KM3NeT, Posicionamiento, Brújulas, Incertidumbres, Calibración, Software

Abstract

The KM3NeT Collaboration is the largest team of scientists and engineers operating the largest deep-sea research infrastructure being built in the Mediterranean Sea, incorporating a network of next-generation neutrino telescopes and devices for multidisciplinary science. KM3NeT is scaling two underwater infrastructures housing large-scale neutrino detectors that share the same technology but with different layouts and scientific targets. These detectors are so-called ORCA (Oscillation Research with Cosmics in the Abyss) and ARCA (Astroparticle Research with Cosmics in the Abyss). ARCA is located at the KM3NeT-It site (Capo, Passero, Italy), and ORCA is in the KM3NeT-Fr site (Toulon, France). The detection principle is based on the recording of Cherenkov light when induced by relativistic charged particles produced in neutrino interactions while crossing the detectors. Each detector comprises a 3D array of Detection Units (DUs) in a modular design. Each DU comprises 18 Digital Optical Modules (DOM), and each DOM contains 31 3-inches PhotoMultiplier Tubes (PMT) responsible for recording the Cherenkov light. Each DOM collects information that allows the reconstruction of the direction, energy range, and timing of neutrino-like events. The detectors work in an all-data-to-shore data transfer mode for the subsequent analysis of this information.

Knowing each DOM's orientation is crucial to determine the directionality of the events of interest in KM3NeT. Within each DOM, specifically in the so-called CLB, a compass board is integrated with a 3D-accelerometer and a 3D-magnetometer, in charge of tilt and orientation readout (*Yaw, Pitch, and Roll*). In addition, an offline calibration procedure was defined for the compass positioning subsystem, identifying the necessary calibration parameters to mitigate uncertainties linked to the device. In this work, the uncertainties estimation for the KM3NeT compass positioning subsystem is studied, and a preliminary parameterization is proposed. As a result, it is verified that the orientation required to meet the KM3NeT physics goals is satisfied: orientation accuracy must be less than 3.5° , essential to guarantee the optimal reconstruction of neutrino-like events from the line-shape reconstruction. The data analysis in this work pointed to an improved orientation accuracy.

Keywords: KM3NeT, Positioning, Compasses, Uncertainties, Calibration, Software

Contents

List of Figures	x
List of Tables	xiii
1 Problem Statement	1
1.1 General and Specific Objectives	2
2 Overview on positioning and off-shore infrastructures	5
2.1 Sea-level Infrastructures	5
2.2 Undersea Infrastructures: KM3NeT	7
2.2.1 Digital Optical Module (DOM)	11
2.2.2 Central Logic Board (CLB)	14
2.2.3 Digital Compasses: accelerometers and magnetometers	14
3 Experimental Methodology	17
3.1 Digital Compasses readout, calibration and YPR reconstruction	17
3.2 On-Site operation and Digital Compasses data selection	21
3.2.1 Data filtering	22
3.3 Digital Compasses performance and systematics	27
3.3.1 The Accelerometer and Magnetometer modulus	28
4 Results and Discussion	31
4.1 Compass data, monitoring and orientation	31
4.2 Compass systematics	36
4.2.1 Compass modulus (accelerometer, magnetometer) and YPR orientation values	38
4.2.2 Preliminary parameterization of Systematic Uncertainties	41
4.2.3 Selection of compasses for online orientation monitoring	45
4.3 Other Contributions to the compass calibration scheme	48
4.3.1 Data Quality from DB	48

4.3.2	Calibration file checks	48
4.3.3	Compass testing in the Dark Room	49
5	Conclusions and Future Work	51
5.1	Conclusions:	51
5.2	Future Work:	52
A	Figures and Tables	53
	Bibliography	63

List of Figures

2.1	Triangulation method in APS. Acoustic receivers of known positions receive omnidirectional signals (red color) generated by an acoustic emitter (<i>i.e.</i> , the cetacean at the center). The method determines the relative distance between emitter-receiver (blue circle). Various receivers allow estimating the absolute position of the emitter ²⁰	6
2.2	Internal Components of the KM3NeT DOM. All the readout, control system, and power supply are managed by the CLB.	8
2.3	The KM3NeT DOM. (a) External view, PMT are clearly visible. (b) Internal view drawing, CLB is seen at the top. (c) CLB electronics top view, in charge of managing all the instrumentation inside the DOM.*	11
2.4	The DOM reference system represented by Cartesian axes centered at "X". (a) Frontal View. (b) Lateral View. (c) CLB and AHRS reference system.*	12
2.5	Yaw (Y), Pitch (P), and Roll (R) angle notation. (a) YPR in DOM reference frame. (b) Any 3D-object orientation can be represented in YPR notation (<i>i.e.</i> plane orientation).	13
3.1	Extract of compass data from the DB, labeled in the DB query.	22
3.2	A sample of duplicated data in ORCA6 compasses (RUN 8501-8550). AHRS-LNS accelerometers representatively shows a greater number of duplicates.	23
3.3	Duplicated entries from a fragment of accelerometer data. A particular case is identified for ORCA6 DU3-F4 (AHRS-LNS model), RUN 7221-7222. Colored boxes enclose the "duplicates" found in different columns.	24
3.4	Duplicates filtering technique for compass data according to Resolution and Communication Effect applied over three different cases (a,b,c).	25
3.5	Some key factors (Calibration, firmware versions) for compasses in ORCA6 regarding data selection in this work.	26
3.6	General scheme for A-H data and uncertainty factors in YPR calculation. The proposed model to reconstruct the YPR values indicates the Y values contain the propagation of the global effects (indirect, direct) of systematic uncertainties.	27
3.7	Acceleration vectors in the global reference system. (a) Acceleration vector in Earth's reference frame. (b) Acceleration vector estimated by compass board (accelerometer).	28

3.8	Magnetic vectors in the global reference system. (a) Earth's magnetic field vector. (b) Magnetic field vector estimated by compass board (magnetometer).	29
4.1	Frequency of recorded events for compass data. (a) Recording frequency histogram. (b) Distribution of compass readout over time.	32
4.2	Reconstructed Pitch (P) values for ORCA6 compasses in Long-Period (includes the Short-Period). Each color represents compass readouts along the DU. Time format: yyyy-mm-dd.	33
4.3	Reconstructed Roll (R) values for ORCA6 compasses in Long-Period (includes the Short-Period). Each color represents compass readouts along the DU. Time format: yyyy-mm-dd.	34
4.4	Reconstructed Yaw (Y) values for ORCA6 compasses in Long-Period (includes Short-Period). Each color represents compass readouts along the DU. Time format: yyyy-mm-dd.	35
4.5	Acceleration vector modulus $ \vec{A} $ estimated by both compass models in ORCA6 Long-Period (except F15). (a) $ \vec{A} $ values for AHRS-LNS in DU9. (b) $ \vec{A} $ values for LSM303 in DU11.	36
4.6	Magnetic vector modulus $ \vec{H} $ estimated by both compass model in ORCA6 Long-Period (except F15). (a) $ \vec{H} $ values for AHRS-LNS in DU9. (b) $ \vec{H} $ values for LSM303 in DU11.	36
4.7	$ \vec{A} $ averaged values overtime for ORCA6 compasses (Long-Period). (a) Heat map: fractions of g by DU and Floor of all DUs (unavailable compasses in black). (b) Fractions of g by Floor and reference value ($ \vec{A} = 1 g$) for DUs detailed comparison.	37
4.8	$ \vec{H} $ averaged values overtime for ORCA6 compasses (Long-Period). (a) Heat map, gauss by DU and Floor of all DUs (unavailable compasses appear in black color). (b) Gauss by Floor and reference value ($ \vec{H} = 0.465 \text{ gauss}$) comparison.	38
4.9	2D orientation distribution of Y (consolidated data selection). (a) Short (Calm) Period dataset. (b) Long-Period dataset.	39
4.10	Mean values for $ \vec{A} $, $ \vec{H} $ and 2D orientation distributions for Yaw (Y) in compasses in ORCA6 for Short (Calm)-Period.	40
4.11	Considerations about DOM orientation. (a) Drag forces diagram acting on DU elements. (b) The individual rotations of a Floor is transmitted to nearby ones, due to cable stretching. (c) Each DOM is fixed in the DU structure by two metallic fibers.	41
4.12	2D orientation distribution for Yaw (Y), Short (Calm) and Long-Period, together Linear Parameterization of Y nominal values (Long-Period) in all ORCA6 DUs. Consolidated data selection is used.	43
4.13	Linear Parameterizations for Y mean-mode values in DU9. (a) Short(Calm)-Period. (b) Long-Period.	44
4.14	Linear Parameterizations for Y mean-mode values in DU11. (a) Short(Calm)-Period. (b) Long-Period.	44
4.15	Error Band representation ($\mathbf{Y}_{\text{data}}(\text{mean}) \pm \mathbf{Y}_{\text{res}} \pm \mathbf{Y}_{\text{data}}(\text{SD})$) and Linear parameterized of \mathbf{Y}_{data} in Long-Period estimated in this work.	46
4.16	Gaussian distributions of reconstructed Y for DU1, DU2, DU3, DU9, DU10 and DU11 in Long-Period dataset of ORCA6.	47

4.17	Interface and outputs of compass data quality script. The script shows by percentage the amount of 0, NaN and raw compass data available in the retrieved dataset.	48
4.18	Interface and outputs of compass calibration file check script. The script easily verifies the sanity of compass calibration files.	49
4.19	Interface and outputs of compass testing script Dark Room setups.	49
A.1	Estimated compass recording frequency for Long-Period, considering all compasses in ORCA6. The recording frequency can be estimated by the time differences mode, calculated as the time difference of consecutive events in the dataset.	54
A.2	Distribution of compass communication data over time for Long-Period, considering all compasses in ORCA6. It is obtained using the UNIXTIME parameter of each compass event recorded in DB. . .	55

List of Tables

1.1	ARCA and ORCA detectors, DU and DOM spacing ¹	2
2.1	General configuration for APS systems. The accuracy of the positioning of an object mainly depends on the number of acoustic emitters/receivers and the layout used ¹⁷	7
2.2	Baseline and DAR elements for APS in KM3NeT. They have been selected accordingly to positioning requirements. DAR receivers have not yet been implemented at detector sites ²⁵	10
2.3	Yaw, Pitch, and Roll (YPR) definition for DOM and global referential system. This rotation angle notation is commonly used to define the orientation of objects and vehicles, in KM3NeT for DOMs analysis rotation ¹	13
2.4	Some technical specs of Digital Compass models available in KM3NeT detectors. The intrinsic features of each Digital Compass model impacts the behavior of the communication and sources of uncertainty ^{36 37 38 39}	15
3.1	Main sources of uncertainties for Accelerometer and Magnetometer sensors ²⁹ . Instrumental uncertainties impact on compass performance, the magnitude of their influence is different for each compass. Additional uncertainties comes from the environment, interfering with the magnetometers performance.	18
3.2	Consolidated uncertainty sources mainly impacting compasses data, according the analytical form of their influence over $\mathbf{A-H}$ vector ³⁰	18
3.3	Compass Data format in the KM3NeT DB. The already developed methods to retrieve compass data can query an specific dataset using these parameters.	21
3.4	Improved data filtering conditions for compass data developed in this work.	25
3.5	Consolidated data selection criteria (cuts/filtering) for compasses data, meaning unbiased inputs towards reasonable systematics study.	26
4.1	$\mathbf{Y}_{\text{data}}-\mathbf{Y}_{\text{res}}$ averaged and $\mathbf{SD}_{\mathbf{Y}_{\text{data}}}^{\text{stat}}$ (Short and Long-Period) and their uncertainties for all ORCA6 DUs.	45
A.1	Mean, Standard Deviation (SD) and Percentage change (%) with respect to the reference values of $ \vec{\mathbf{A}} $ and $ \vec{\mathbf{H}} $ (fractions of g and $gauss$ respectively) for ORCA6 compasses in Long-Period.	56

A.2	$Y_{\text{data}}(\text{mean})$, $Y_{\text{data}}(\text{SD})$ and $Y_{\text{data}}(\text{mode})$ in estimated from compass data in Short-Period . All quantities are represented in degrees.	57
A.3	$Y_{\text{data}}(\text{mean})$, $Y_{\text{data}}(\text{SD})$ and $Y_{\text{data}}(\text{mode})$ in estimated from compass data in Long-Period . All quantities are represented in degrees.	58
A.4	Y_{res} for DU1 in Short-Period (RUN 8000-8085). All quantities are represented in degrees.	59
A.5	Y_{res} for DU2 in Short-Period (RUN 8000-8085). All quantities are represented in degrees.	60
A.6	Y_{res} for DU3 in Short-Period (RUN 8000-8085). All quantities are represented in degrees.	60
A.7	Y_{res} for DU9 in Short-Period (RUN 8000-8085). All quantities are represented in degrees.	61
A.8	Y_{res} for DU10 in Short-Period (RUN 8000-8085). All quantities are represented in degrees.	61
A.9	Y_{res} for DU11 in Short-Period (RUN 8000-8085). All quantities are represented in degrees.	62

Chapter 1

Problem Statement

The KM3NeT Collaboration is the largest team of scientists and engineers building and operating an undersea research infrastructure in the Mediterranean Sea, incorporating the next generation neutrino telescopes network, multidisciplinary and multipurpose. As of February 2020, KM3NeT Collaboration comprises 56 institutes and groups in 48 cities in 17 countries along four continents*. Multidisciplinary programs include Physics, Earth and Sea Science, *i.e.* monitoring seafloor and marine life. Physics programs are focused on the study of extraterrestrial Neutrino sources, the Neutrinos Mass Hierarchy (NMH), and the CP leptonic phase¹. In addition, KM3NeT offers long-term monitoring since permanent connections (powering and readout instruments) to shore. Although it is not yet in its final stage of construction, KM3NeT is projected as a world-leading observatory with enormous discovery potential (ESFRI^{2,3} and LASF4RI⁴ roadmaps), being also an important node in a global neutrino and undersea observatories. KM3NeT is scaling two neutrinos detectors with well-defined purposes, following a modular design to keep operational while construction. These detectors are ORCA, densely configured to detect atmospheric neutrinos, and ARCA optimized to detect high-energy neutrinos. ARCA is being implemented at the KM3NeT-It site (Capo Passero, Italy), at 3500 m depth, and ORCA at the KM3NeT-Fr site (Toulon,France), at 2500 m depth¹. Detectors differ in their layout but share the same technology. Both detectors are based on the Cherenkov radiation detection, induced by relativistic charged particles that emerge from neutrino interactions. The design of the KM3NeT infrastructure offers the possibility of studying neutrinos and monitoring the ocean floor and marine life. Each detector is made up of building blocks, a building block comprises 115 Detection Units (DUs). Each DU is anchored to the seabed and vertically houses 18 Digital Optical Modules (DOMs). The vertical and horizontal arrangement of the DOMs depends on the detector layout, as summarized in Table 1.1. The DOM is the Cherenkov sensitive frontier, each containing 31 3-inches PhotoMultiplier Tubes (PMT), collecting the intensity, timing and direction of light in the vicinity of the DOM.

*<https://www.km3net.org>

Detectors Configuration (KM3NeT Phase-II)		
	ARCA	ORCA
Number of Building Blocks (115 DUs)	2	1
Average Separation between DUs [m]	95	20
Total Length of DU (vertical direction) [m]	700	200
Space between DOMs [m]	36	9
Distance of the first DOM with respect of the seabed [m]	80	40

Table 1.1: ARCA and ORCA detectors, DU and DOM spacing¹.

To reach the KM3NeT physics goals, concerning positioning and orientation (this work) requirements, a DOM positioning < 20 cm and orientation accuracy $< 3.5^\circ$ need to be reached. In this sense, an Acoustic Positioning System (APS) has been implemented to provide accurate positioning data, using acoustic transmitters and receivers to determine the DOM position in a geo-referenced field⁵. Concerning sea current affecting the detectors elements positioning, DOMs experience two types of movements: translation and rotation. It is expected that the greater the intensity of the sea current, the greater the influence on DOM positioning. Specifically, a positioning subsystem called the Attitude Heading Reference System (AHRS) board has been included inside each DOM to act as the “compass” system. The compass board, installed in the Central Logic Board (CLB), consists of a 3D-accelerometer and a 3D-magnetometer which determine the tilt and orientation data for each DOM⁶. The compass system collects raw data; then, this raw data must be calibrated (offline calibration for each compass^{6,7}). An improved uncertainties analysis must be done looking to upgrade the available compass calibration scheme (the essence of this work).

1.1 General and Specific Objectives

As general, this work, aims to evaluate the Digital Compasses performance in KM3NeT and carry out a dedicated analysis of systematics, based on the following specifics:

- Establish improved filtering conditions for compass data.
- Performs compass data communication sanity checks.
- Study the accelerometer and magnetometer vector modulus from digital compasses, and get insights about orientation uncertainties of the DOM and its stability in time.
- Estimation of Yaw (Y) as representative magnitude for orientation assessment for several periods of ORCA detector and assumption of external effects conditions (horizontal and vertical drag forces by sea current).
- Parameterization of Nominal Y values, accounting for statistical and associated systematics uncertainties.

- Verify the DOM orientation accuracy required for the successful reconstruction of directionality of neutrino-like events is $< 3.5^\circ$.

Applications beyond experimental High-Energy Physics (HEP). Digital Compasses are not limited to undersea neutrino observatories. Compass orientation principles are shared with most commonly known geolocation systems, i.e. the behavior and conditions found in the Global Navigation Satellite System (GNSS)⁸. GNSS is based on a network of satellites (of known position) with synchronized clocks⁸, similar to the positioning and timing procedure applied in KM3NeT. Specifically, the transmission of the signal from at least three satellites allow calculating the distances concerning a signal receiver is referred to as triangulation technique⁹, the same principle applied with the APS implemented in KM3NeT. The main difference between GPS and APS is that the radio frequency attenuation (used by GPS¹⁰) is very high in marine environments. Implementing an APS is more effective, whose attenuation is much lower using triangulation principles and positioning of underwater structures. Another innovative positioning technique is the space positioning, *i.e.* NASA's Jet Propulsion Laboratory developed the "Positioning System in Deep Space", based on optical navigation using a camera system to determine a vehicle relative position or orientation to the Earth¹¹. Another example comes from SpaceX, Starlink project¹² expected to deploy a network of 4,425 satellites in low Earth orbit to increase internet bandwidth integrating complex communication and relative positioning systems¹³. Along with APS and GNSS-based reference systems, it is common to implement orientation systems with technology similar to the compass system implemented in the KM3NeT infrastructure¹⁴. Although the orientation systems implemented in satellite positioning do not depend directly on the Earth's magnetic field, all the orientation systems, regardless of the technology used, depend on referential systems projection to a global reference system. In the case of SpaceX satellites, they integrate the relative positioning system information and takes advantage of the instrumentation present in the satellite¹². Similarly, the relative positioning systems (APS and compasses) data from each KM3NeT DOM allow positioning to a global reference system (Earth reference frame). A typical application case of this technology comes from smartphones: the uncertainties of this technology orientation are closely related to the nature of the materials integrated into the device¹⁵.

Chapter 2

Overview on positioning and off-shore infrastructures

Back in history, positioning started when humanity began to navigate the seas taking as reference the coastlines. Then, the reference system became the sky stars, a known star is identified, then the angle to the horizon is estimated. It was then possible to determine the region and orientation of a navy¹⁶. The development of this positioning at the beginning of navigation science set the basis of modern navigation tools concerning GPS¹⁰ and APS-based¹⁷. Positioning is defined as the process of determining the precise physical location of objects, vehicles, ships, people or places, at a particular point in time¹⁸. The available positioning systems and models offer different performances depending on the number of objects to be positioned, the absolute-relative positions, and environmental conditions. In general, any positioning method is based on referencing the relative position of an object of interest to a known object position (fixed or not)¹⁷ coordinates.

2.1 Sea-level Infrastructures

For navigation and underwater communications, acoustic transmission systems are primordial. An acoustic system works by exchanging acoustic signals among the implemented system components. The transmission of these acoustic signals is determined by factors such as the sound speed in the medium, the configuration of components, specification of the electronics, and other environmental conditions. The marine environment factors interfere with an acoustic signal when propagating. An acoustic signal is distributed in different directions, depending on temperature, pressure, and salinity factors. It is possible to identify an acoustic signal pattern over the acoustic background in the environment. The greater the distance traveled by the acoustic signal, the lesser the intensity because a fraction of the signal energy is absorbed by the water. These conditions for the transmission of acoustic signals are considered in the development of underwater positioning systems. An APS is based on the acoustic signal exchange between emitters (*e.g.* transducer) and receiving elements (*e.g.* hydrophones). Commonly, the

acoustic emitters are piezoelectric elements. The piezoelectric element receives a pressure (mechanical) wave, then this signal is converted in electrical pulses¹⁹. In this way, acoustic positioning is based on the propagation of acoustic signals produced by known position devices. When these acoustic signals are received, it is possible to determine the relative position of the place where this signal is received, concerning the emitting devices, this process is called Triangulation¹⁸, as illustrated in Figure 2.1. This method considers certain environmental factors to determine the positioning accuracy, being density the most crucial factor. The density of the water affects the speed at which sound can travel. An accepted value for the speed of sound in salt water is ~ 1500 m/s. However, an improvement in accuracy is reached with additional information about the environment, such as water temperature and salinity conditions²⁰.

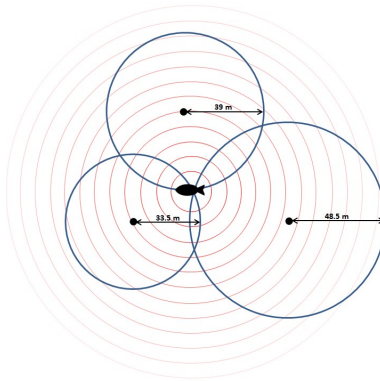


Figure 2.1: Triangulation method in APS. Acoustic receivers of known positions receive omnidirectional signals (red color) generated by an acoustic emitter (*i.e.*, the cetacean at the center). The method determines the relative distance between emitter-receiver (blue circle). Various receivers allow estimating the absolute position of the emitter²⁰.

In general, the APS uses acoustic pulses sources/receivers to determine the wished object location, which acts as an acoustic receiver/emitter. The distance between the emitter and receiver is calculated according to the time in which the pulse was produced, and the time it was received. The position obtained is relative to the devices that generate the acoustic pulses. In APS, the most used devices to act as acoustic transmitters at fixed locations are transducers that generate acoustic signals (sound pulses) commonly traveling omnidirectionally. Hydrophones are standard acoustic detection devices, while the beacons act as acoustic emitters. Once the distances from the beacons and hydrophones are known, it is possible to determine the device location in a geo-referenced field. In this way, the APS allows positioning and tracking in the water of ROV (Remote Operated Vehicles), AUV (Autonomous Underwater Vehicles), and sensors located in the seabed. In the same way, APS is useful for transfer of position from the surface to the seabed (*i.e.* drilling and installations on the seabed of oil sites) and relative positioning of sea creatures (used in multidisciplinary submarine observatories as KM3NeT). An APS-based technique is more convenient than a radio-based technique in undersea environments. Radio signals are absorbed by water easily, creating a limitation for implementing GPS-based methods in underwater environments¹⁷. The specific configuration of acoustic emitters/receivers implemented characterizes the type of APS choice. A general classification of these

positioning systems is shown in Table 2.1.

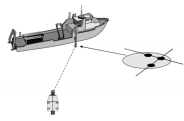
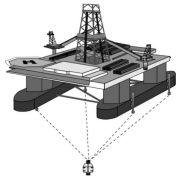
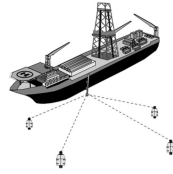
Types of Acoustic Positioning Systems (APS)		
<p>Ultra Short Baseline (USBL)</p> <p>Determines beacon position by measuring the relative phases of the acoustic signal received by closely spaced elements in a single hydrophone.</p> <p>Advantages:</p> <ul style="list-style-type: none"> • Low system complexity. • Single acoustic transmitter (beacon). <p>Disadvantages:</p> <ul style="list-style-type: none"> • Absolute position accuracy depends on additional sensors. • Detailed calibration of system required. 	<p>Short Baseline (SBL)</p> <p>Determines beacon position by measuring the relative arrival times at three or more vessel-mounted hydrophones.</p> <p>Advantages:</p> <ul style="list-style-type: none"> • Low system complexity • Improved accuracy over USBL. <p>Disadvantages:</p> <ul style="list-style-type: none"> • Absolute position accuracy depends on additional sensors. • Detailed calibration of system required. 	<p>Long Baseline (LBL)</p> <p>Determines beacon position by measuring the slant ranges from three or more widely spaced acoustic transmitters (beacon).</p> <p>Advantages:</p> <ul style="list-style-type: none"> • Very good position accuracy independent of water depth. • High relative accuracy positioning over large areas. <p>Disadvantages:</p> <ul style="list-style-type: none"> • Complex System. • Large arrays of expensive equipment. 

Table 2.1: General configuration for APS systems. The accuracy of the positioning of an object mainly depends on the number of acoustic emitters/receivers and the layout used¹⁷.

2.2 Undersea Infrastructures: KM3NeT

Acoustic positioning applied to underwater observatories is a special challenge. Considering a particular case, the ANTARES Neutrino Observatory was designed with 12 vertical strings separated by 70 m between them, located 40 km offshore Toulon (France) at 2500 m depth. Each string comprises 75 Optical Modules (OM) arranged in triplets by storey²¹, each housing single large-area PMTs and a Local Central Module (LCM) just above. The strings are anchored to the seabed and maintained vertically by a buoy, similar as in KM3NeT. The strings are not fixed, then positions of the OMs can be drifted by water current flows. ANTARES demands accuracy of the OM better than 20 cm for positioning, ~ 1 ns for timing, and a few degrees for orientation²¹. An APS based on an LBL was implemented in ANTARES. This LBL monitors the signals sent by the five hydrophones distributed in each string in a non-uniform way considering only the most strategic points. The APS also integrates a transponder (acoustic transmitter/receiver) at the base of each string, accompanied by autonomous transponders in the sea floor²². Hence, the position of elements in the infrastructure is determined by acoustic triangulation concerning fixed emitters in

the seabed. Additionally, the APS is complemented with the information provided by the compass–tiltmeter system mounted on each storey, this system gives the local measurements of tilt and heading^{21 22}. ANTARES plus other undersea neutrino observatories prototypes set a precedent for developing the next generation neutrino observatories to be constructed this decade: Baikal-GVD²³, P-ONE²⁴, and KM3NeT.

In the case of KM3NeT, the detector layout is composed of Building Blocks (Table 1.1). The Building Blocks are connected to the shore station, following all-data-to-shore data transfer mode. The shore station is responsible for the power supply and connects the undersea infrastructure readouts with a PC farm, responsible for loading and filtering the information collected. Each DOM collects information about the direction and energy of the Cherenkov light detected in its vicinity, furthermore these optical data, positioning, and orientation data, among others. In the DOM, the main processing unit is the Central Logic Board (CLB). Each CLB houses different elements capable of ordering, labeling, and transmitting the PMT data to the shore station. All the CLBs are controlled by the Detector Manager (DM) at the software level. As seen in Figure 2.2, each DOM is surrounded by a 17-inch high-pressure resistant glass sphere, innermost a plastic structure that fixed the 31 PMTs position, along with all the electronics, calibration devices including those for positioning and orientation.



Figure 2.2: Internal Components of the KM3NeT DOM. All the readout, control system, and power supply are managed by the CLB.

The DU structure and DOM designs favor stability, moreover, the buoyancy in the top of the DU structure gives an extra flotation mechanism to avoid collapse and reduce sudden horizontal movements¹. At ideal conditions (*i.e.* negligible ocean currents), the mechanical position of the DU elements is unaltered (nominal position). In default conditions, sea currents displace the structures of their nominal position, and the DOMs experience rotations. In

KM3NeT, two APS have been implemented to determine key parameters for the line shape reconstruction and satisfy the observatory scientific goals. The APS for ARCA and ORCA detectors are composed of two subsystems: 1) baseline of acoustic transmitters (beacons) and receivers located at known positions, and 2) an array of Digital Acoustic Receivers (DARs) installed along the DUs. An On-Shore acoustic data analysis software is run to interpret and filter the acquired positioning data⁵. Currently, not all the elements of each subsystem are implemented in the detector sites. The integration of these devices is taking place gradually.

Deployment of DUs and NAAPS. The absolute position of the baseline elements is determined by the Navigation and Absolute Acoustic Positioning System (NAAPS), NAAPS geo-reference deployment position of baseline elements¹ accordingly to each detector APS configuration. For ORCA, it is planned to implement a LBL system, for ARCA, an USBL. The absolute position of the structures in the detector can be determined using the baseline elements absolute position. This absolute positioning can be verified by identifying the arrival position using external instruments (*i.e.* ROV vehicle). NAAPS is expected to obtain the absolute geo-referenced position of the bases of each deployed DU. In general, it has been estimated that the accuracy of the position offered by the NAAPS varies ~3 m concerning the actual position of the deployed element on the sea floor⁵. The baseline elements position at the ARCA and ORCA sites has to be known in the same order at which it is necessary to know the DOM position⁵, an accuracy better than 20 cm is mandatory. An iterative algorithm has been designed to recalculate each baseline element position, improving the position accuracy. The algorithm considers the absolute position provided by the NAAPS, accounting there are an hydrophone and an acoustic emitter installed in the same mechanical structure, expected to be integrated with each DU base. Additionally, with the amount of "autonomous" acoustic emitters deployed in strategic places, the algorithm can estimate the necessary corrections to the absolute position provided by NAAPS for each baseline element. This estimation considers each baseline element fixed at a relative distance, and compares these relative distances to calculate the associated residuals. For this, it is necessary to take into account the Time of Emission (ToE) and Time of Arrival (ToA) of the acoustic signals emitted, the calculation of the relative distances is also possible knowing the speed of sound *in-situ*. At the moment, this iterative algorithm is partially operational in the KM3NeT integration state, considering only autonomous emitters²⁵.

Operative conditions of the DUs. The acoustic position at first instance depends on the position obtained by the NAAPS, which then allows determining the position of each DOM using the Relative Acoustic Positioning System (RAPS) system. The DARs acquire all the acoustics signal emitted, distributed throughout the detector layout with two purposes. An iterative algorithm uses External DAR (digital hydrophones) elements data to calibrate the baseline position by measuring the relative distance among baseline elements. Additionally, internal DAR elements (piezoelectric glued inside the glass sphere of DOM) are used to calculate the relative position of each DOM to the baseline elements, allowing to monitor the movements of the DUs due to underwater currents²⁵. The features of the baseline and DARs elements in KM3NeT are shown in Table 2.2.

The frequency at which acoustic transmitters emit a signal typically is in the 20-40 kHz range to properly propagate through the water at the detector volume²⁵. The acoustic data collected by acoustic receivers are sent to the shore

station for analysis. The shore station includes a PC farm that analyzes the data allowing to obtain the DOM position through multiple triangulation²⁶. It is considered that the primary source of uncertainty of the APS implemented in the KM3NeT is the errors in the baseline relative position elements. The main challenge when applying corrections is to precisely determine the acoustic disturbances or proper calibration of the DAR and baseline elements^{25,5}. The information provided by APS can be used to detect and monitor external sources of noise pollution, such as marine vessels, tracking and detecting of cetaceans²⁷, even to analyze correlations between acoustic and optical signals while detecting High-Energy neutrino interactions²⁸. Complementing the APS, a Digital Compasses system is responsible for measuring the orientation and tilt of the DOM, complemented by pressure, current, and sound velocity devices.




External Digital Acoustic Receiver (DAR)	Acoustic emitters	Internal Digital Acoustic Receiver (DAR)
<ul style="list-style-type: none"> • Model DG0330. • Spherical piezo-ceramic element along with an analogue board. • Calibrated in pressure sensitivity and directionality. • Calibrates baseline elements. 	<ul style="list-style-type: none"> • Model SX30. • Can be reconfigured for <i>in-situ</i> optimization of the signal detection. • Synchronized with the detector master clock. • Can operate autonomously. 	<ul style="list-style-type: none"> • Model not defined. • Destined to monitor the DU movement under sea currents and allow line reconstruction. • Allows RAPS implementation.
<p>Location: DU Anchor Base.</p>	<p>Location: DU Anchor Bases and Strategic Locations.</p>	<p>Location: Glued from the inside to “south pole” of the glass sphere of each DOM.</p>
		

Table 2.2: Baseline and DAR elements for APS in KM3NeT. They have been selected accordingly to positioning requirements. DAR receivers have not yet been implemented at detector sites²⁵.

Digital Compasses operation. Although the first compasses were initially based on magnetic materials, the technologies used for orientation have improved over time, leading to Digital Compasses. Digital Compasses do not require magnetic materials to determine the direction of the Earth’s magnetic field. The reliability of the orientation obtained depends on the configuration of sensors implemented in the compass. In general, a Digital Compass integrates a magnetometer to estimate the Earth’s magnetic field and an accelerometer that estimates the acceleration field’s intensity. The magnetometer contains an Anisotropic Magnetoresistive Sensor (AMS). This sensor estimates the Earth’s magnetic field’s ultra-low frequency signals coming from the North or South direction, estimating the field’s orientation, direction, and intensity. In the accelerometer case, the sensor contains a Micro Electro-Mechanical

System (MEMS) in charge of estimating the angle between the compass reference system and the horizontal plane, estimating the intensity and direction of the acceleration field. The magnetometer is responsible for estimating the orientation (Yaw). In contrast, the accelerometer estimates the inclination (Pitch and Roll) concerning the horizontal plane in the compass reference system^{29,30}. In KM3NeT, each DOM has an independent orientation system consisting of a custom Digital Compass integrated in the CLB. Moreover, each compass contains: a 3D-accelerometer and a 3D-magnetometer, estimating the acceleration field vector and the magnetic north's deviation, respectively. The CLB receives accelerometers and magnetometers data from the compass board. Then, compass data is sent to the shore station for filtering and long-term storage and analysis. The data collected by this system is essentially raw. The calibration procedure (offline) finds the calibration parameters needed to properly reconstruct the orientation²⁵. The technology used for DOM orientation is the same implemented in most systems that depend on the Earth's magnetic field. The 3D-accelerometer and 3D-magnetometer collects the necessary information to calculate the orientation parameters, which in the case of this work correspond to Yaw (Y), Pitch(P), and Roll (R) notation (YPR), most common aeronautical rotational description³¹.

2.2.1 Digital Optical Module (DOM)

To properly reconstruct neutrino events concerning positioning and orientation, the DOM coordinates frame is defined as the reference system for the 31 PMTs inside the DOM. The PMTs are physically fixed in a support structure inside the DOM, so each PMT has fixed coordinates in the DOM reference frame. Figure 2.3 illustrates DOM external view and the main inner components³².

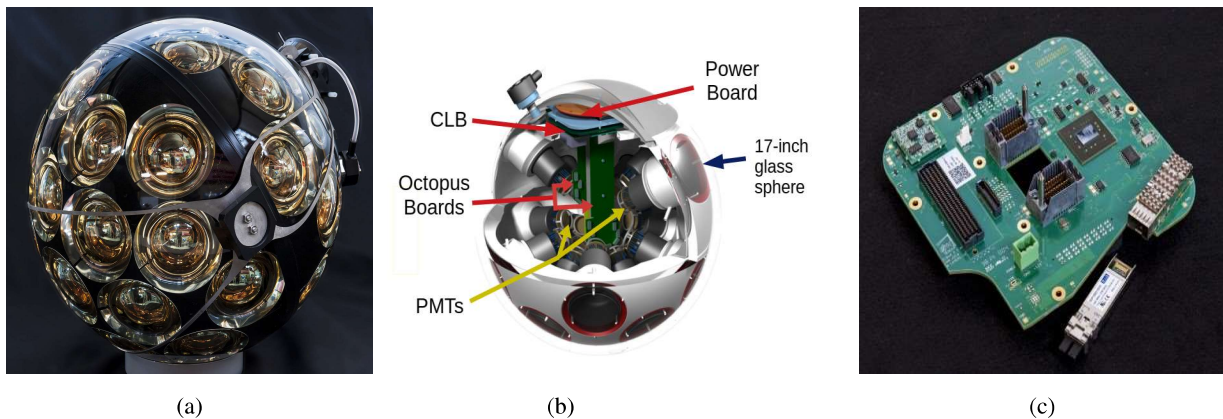


Figure 2.3: The KM3NeT DOM. (a) External view, PMT are clearly visible. (b) Internal view drawing, CLB is seen at the top. (c) CLB electronics top view, in charge of managing all the instrumentation inside the DOM.*

The DOM reference frame shown in Figure 2.4 can be translated to a global reference system. For this purpose, it is required to know each DOM orientation definition and position with respect to a global reference.

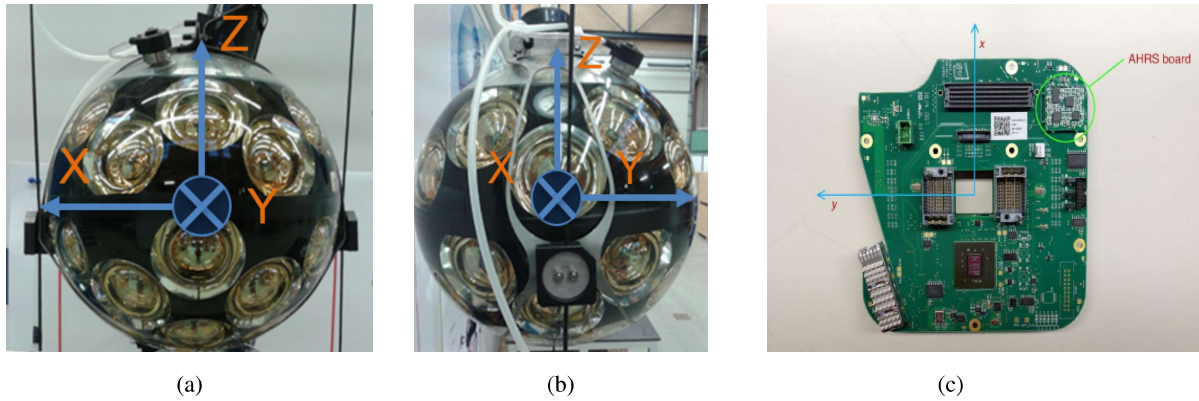


Figure 2.4: The DOM reference system represented by Cartesian axes centered at "X". (a) Frontal View. (b) Lateral View. (c) CLB and AHRS reference system.*

To determine the orientation of each DOM in the global referencing system, the CLB³³ (Figure 2.3c) reference system aligns with the DOM's reference system. Additionally, it must be taken into account that the CLB board is mounted upside-down, then, all compass data on the z-axis has the opposite sign. The cartesian reference system of the DOM, CLB, and compass are equivalent. The compass board is located in one of the corners of the CLB, when calculating the orientation, it is equivalent to the same as the CLB³³. The notation used to represent the orientation from compass data is based on YPR angles representation, as illustrated in Figure 2.5. YPR angles representation was routinely used to represent the orientation of rigid bodies in aerospace, navigation, and robotics³¹. A general object in 3D can be rotated around its 3 orthogonal axes. Thus, YPR represents the rotation angle around the former z-axis, the angle of rotation around the formerly y-axis, and the angle of rotation around the x-axis. DOM orientation is projected in the global reference frame (Earth magnetic field and total Earth acceleration field). In the DOM reference system, x-axis points to the geographical North and the y-axis points to the geographical East¹.

* The photos contained in this section were obtained from a private database of the KM3NeT collaboration.

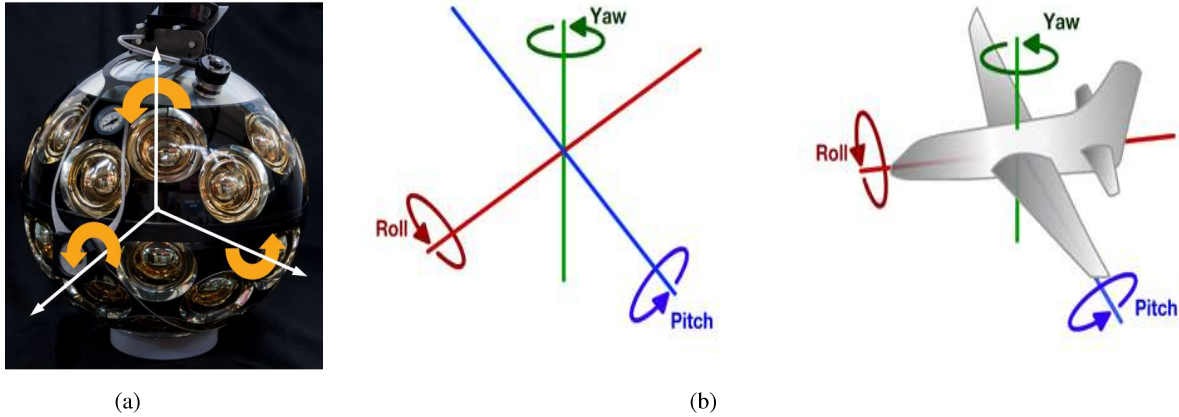


Figure 2.5: Yaw (Y), Pitch (P), and Roll (R) angle notation. (a) YPR in DOM reference frame. (b) Any 3D-object orientation can be represented in YPR notation (*i.e.* plane orientation).

In Table 2.3, the YPR notation is further explained for the DOM reference system and the global reference system used in this work.

Yaw Angle Rotation	Pitch Angle Rotation	Roll Angle Rotation
<ul style="list-style-type: none"> • Angle of the DOM +x-axis with the magnetic North in the global reference frame. • Angle of rotation of the DOM around its z-axis from +x-axis to +y-axis. • Varies between $[0,360]^\circ$. 	<ul style="list-style-type: none"> • Angle of the DOM +y-axis with the horizontal in the global reference frame. • Angle of rotation of the DOM around its +y-axis from +z-axis to +x-axis. • Varies between $[-90,+90]^\circ$. 	<ul style="list-style-type: none"> • Angle of the DOM +x-axis with the Magnetic East (horizontal) in the global reference frame. • Angle of rotation of the DOM around its +x-axis from +y-axis to +z-axis. • Varies between $[-90,+90]^\circ$.

Table 2.3: Yaw, Pitch, and Roll (YPR) definition for DOM and global referential system. This rotation angle notation is commonly used to define the orientation of objects and vehicles, in KM3NeT for DOMs analysis rotation¹.

2.2.2 Central Logic Board (CLB)

The most representative DOM control systems are: octopus boards (used to gather signals from PMT bases), a power board (supply all the voltage needed by the CLB), and the primary control and readout system within the DOM: the CLB^{34,35}. In the all-data-to-shore data transfer model implemented in KM3NeT, each DOM is a "node" integrated into the KM3NeT detector's communication network. Each CLB is responsible for synchronizing all nodes of this network with the master clock (on the shore station), organizing and labeling the suitable timestamp to the digitized readouts from integrated devices. Moreover, the CLB controls: compass, tiltmeter, piezoelectric sensor, LED nanobeacon, and temperature sensor³⁴.

- **Hardware.** The CLB has several integrated components, the main one being the FPGA, where all the reading and instrumentation functionalities are implemented. The FPGA stores four firmware images, three of which are reconfigurable. The non-reconfigurable image (also called the golden image) provides a safe boot in case of corruption of the reconfigurable images. The CLB can boot with any of this four firmware images³⁴.
- **Firmware.** The CLB firmware is based on two LM32 microprocessors. One of them integrates the necessary protocol to achieve sub-nanosecond synchronization with the master clock. The second one accesses the communications of all the devices integrated into the DOM (*e.g.*, instrumentation devices and optical/acoustic reading systems). The CLB readouts are sent to the shore station³⁴.
- **Software.** A complex and robust software running on the LM32 microprocessors controls the DOM operations. This software contains three layers: 1) communication layer dedicated to basic functions, 2) platform layer includes the necessary drivers, and 3) layer of application that includes the specific codes that contain the necessary configurations for the control of the devices integrated into the DOM (optical/acoustics reading systems)³⁴.

2.2.3 Digital Compasses: accelerometers and magnetometers

To determine the tilt (PR) and the heading (Y), a Digital Compass has been implemented in each DOM. This compass, formed by an accelerometer and magnetometer, allows estimating the orientation with respect to geo-referenced fields, Earth magnetic field, and total accelerating vector, as commented before. Currently, two Digital Compass models have been implemented in ARCA and ORCA detectors, as listed in Table 2.4. The oldest model, called AHRS-LNS, is operative since 2017/09/22 (deployment of ORCA DU1), and a new compass model called LSM303, since 2020/01/26 (deployment of ORCA DU7). Each compass model shares the same objective but has different technology, their electronic features are closely similar, but a different impact on data recorded.

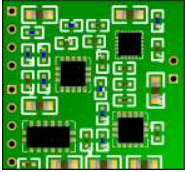

Compass models in ARCA and ORCA detectors					
AHRS-LNS			LSM303		
					
LIS3LV02DL 3D accelerometer and HMC5843 3D magnetometer in separated chips.			3D accelerometer and 3D magnetometer sensor integrated in a single custom chip.		
	Accelerometer	Magnetometer		Accelerometer	Magnetometer
Range	± 2 g	± 4 gauss	Range	± 2 g	± 2 gauss
Resolution	< 1 mg	< 7 mgauss	Resolution	N/A	< 2 mgauss

Table 2.4: Some technical specs of Digital Compass models available in KM3NeT detectors. The intrinsic features of each Digital Compass model impacts the behavior of the communication and sources of uncertainty^{36 37 38 39}.

In agreement to Table 2.4, the range corresponds to the sensor absolute maximum value, which depends on the operating mode configured for each sensor. On the other hand, the resolution is the least significant amount that the sensor can reliably represent. Additional features such as nonlinearity, sensitivity, etc., are available in the technical data sheets provided for each compass model^{37 38 39}. Both compasses have similar features, then similar performance is expected. The older compass model (AHR-LNS) consists of a board built with the commercial sensors LIS3LV02DL (accelerometer) and HMC5843 (magnetometer), both from different suppliers. Preliminary studies in KM3NeT determined that the behavior of the AHRS-LNS satisfies technical requirements³⁶, as the expected both sensors provide reliable data. However, the behavior of the data stream may be different. In the case of the LSM303 compass, sensors are integrated into a single chip modified to meet the requirements of KM3NeT. LMS303 is the most recent model and has an improved performance over the former one.

The instrumental features of each compass model represent different conditions that affect both the data stream and compass data quality. An analysis of these features is necessary to understand the compasses behavior and the influence of systematic uncertainties.

Chapter 3

Experimental Methodology

This work started by collecting technical and experimental information concerning the state of the art of the Digital Compasses operation in KM3NeT. Afterwards, the experimental methodology is followed by the dedicated analysis on the digital compasses readout, cross-checks or fundamental calibration aspects and how the orientation is reconstructed from YPR parameters. Looking forward to the robustness of the experimental methodology, a special data selection is proposed aimed to a promising systematics study to be improved in the near future, for compass data, and started in this work.

3.1 Digital Compasses readout, calibration and YPR reconstruction

Two models of compasses are in charge of the DOM orientation in KM3NeT: AHRS-LNS and LSM303. Each model implements a 3D-magnetometer (3-axis) and a 3D-accelerometer (3-axis), estimating the geomagnetic and gravitational field respectively²⁹. The accelerometer and magnetometer sensors data are used for the reconstruction of the YPR rotation angles. The technology implemented in the AHRS-LNS and LSM303 models is widely used in orientation devices. Such devices share common sources of instrumental uncertainties from the intrinsic nature of their constituent materials and the method of construction³⁰, as summarized in Table 3.1. The accelerometers and magnetometers instrumental uncertainties propagate to the reconstructed YPR orientation values. The default analytic method to reconstruct YPR and the compass calibration method (offline) were developed by KM3NeT previous to this work. The work done in this thesis goes beyond, and explores some unidentified behavior of compasses and discusses the calibration methods (offline) implemented for the KM3NeT compasses.

Accelerometers/Magnetometers electronics contributions	
Offset Error:	Instrumental deviation of zero prior in the in the absence of any field.
Cross Axis Sensitivity Error	Combination of alignment errors, etching inaccuracies and circuit crosstalk.
Sensor noise	Error related with nature of measurements.
A/D converter resolution	The Analog-to-Digital conversion defines the resolution of the measurement.
Temperature effects	Temperature affects the nature of the sensor components.
Magnetic fields contributions	
Hard iron errors	Caused by a magnetic source with permanent field, generate a bias in the sensed field for magnetometers.
Soft Iron Errors	Caused by ferromagnetic materials. These magnetic fields have a direct relationship with the Earth's magnetic field. Orientation-dependent perturbations that create scale errors.

Table 3.1: Main sources of uncertainties for Accelerometer and Magnetometer sensors²⁹. Instrumental uncertainties impact on compass performance, the magnitude of their influence is different for each compass. Additional uncertainties comes from the environment, interfering with the magnetometers performance.

The accelerometers and magnetometers data can be generally represented in vector notation as seen in Equation 3.1.

$$\text{Compass data} \Rightarrow \left\{ \begin{array}{l} \text{Accelerometer} \Rightarrow \mathbf{A} = \begin{pmatrix} A_x \\ A_y \\ A_z \end{pmatrix}, \text{ Magnetometer} \Rightarrow \mathbf{H} = \begin{pmatrix} H_x \\ H_y \\ H_z \end{pmatrix} \end{array} \right. \quad (3.1)$$

The uncertainties associated with raw data of compasses are propagated to accelerometer and magnetometer data in matrix or vector form. Based on Table 3.1, uncertainties for compasses data can be better represented by 4 categories according to the effects over accelerometer/magnetometer vectors as shown in Table 3.2.

Uncertainty	Explanation
Offset Errors	Compass measurement in vector notation is shift by a constant vector value with respect the real one.
Scale Factor Errors	Instrumental errors or environmental factors affect the scale at which each sensor axis measure.
Non-Orthogonal Errors	Three axis of the sensor may not be orthogonal due to manufacturing defects.
Misalignment Errors	The axes of the sensor (accelerometer/magnetometer) are not always aligned with the axes of the compass board on which they are mounted.

Table 3.2: Consolidated uncertainty sources mainly impacting compasses data, according the analytical form of their influence over $\mathbf{A-H}$ vector³⁰.

Specifically, the analytical form of the corrections for Scale Factor, Non-Orthogonal, and Misalignment Errors can be represented as a matrix. On the other hand, the analytic form of the corrections for Offset Errors can be simply a vector^{29 30}. The matrix-vector corrections components depend on the implemented technique and the compass features. Before the DOMs integration in the DUs, a calibration procedure is carried out on all the implemented compasses, an improved strategy over time performed in the different integration sites. Two calibration procedures have been developed so far: 1) Plane Calibration and 2) Wobbling Calibration.

Plane Calibration

- **Accelerometers (A).** The AHRS board (implemented in the CLB) is held horizontally on a suitable horizontal surface to be the test bench (*e.g.* table/desk), accelerometer data are recorded during ~ 2 minutes. In this case, the values of \mathbf{A}_x and \mathbf{A}_y should be close to 0, and their offsets ($\mathbf{A}_{x_{\text{off}}}$ and $\mathbf{A}_{y_{\text{off}}}$) can be obtained from the average of the values of \mathbf{A}_x and \mathbf{A}_y taken during this time. The $\mathbf{A}_{z_{\text{off}}}$ can be determined if the CLB board is vertically placed in the test bench position and performing the same procedure. Depending on the selected position, an equivalent $\mathbf{A}_{y_{\text{off}}}$ or $\mathbf{A}_{x_{\text{off}}}$ is obtained equivalent to the previously calculated value. Preliminary studies in KM3NeT⁶ showed that the maximum tilt experienced by the DOM in the underwater environment is $< 10^\circ$. When increasing the tilt (PR) more than such value, uncertainties on Y becomes more representative⁶.
- **Magnetometers (H).** In the presence of a uniform magnetic field, the values of \mathbf{H} recorded while rotating the CLB in 3-dimensions must correspond to a perfect sphere centered at the origin if placed in a Cartesian representation, under uncalibrated conditions, a spheroid is obtained. In the presence of hard magnetic materials (field independent on the external field), the sphere is shifted concerning the origin (0,0 system of coordinates of the magnetometer). In the presence of soft magnetic materials (field dependent on the external field), the sphere is deformed (ellipsoid). Previous studies in KM3NeT determined that the influence of soft magnetic materials is negligible⁷, therefore, the offset errors are the most representative. The magnetometer offsets (\mathbf{H}_{off}) are determined from the spheroid representation. To obtain the offsets, the CLB is rotated in 6 different planes. For each plane, an ellipse is obtained, a fit is made on its contour to determine the displacement to the origin (0,0 system of coordinates of the magnetometer), the offsets of the plane's axes are obtained. When considering 6 planes, a comparison can be made with all the parameters obtained.

In this way, the Plane Calibration for Digital Compasses runs over the offset corrections only (\mathbf{A}_{off} and \mathbf{H}_{off}). Studies of compasses performance in different conditions⁶ show the calibration effectiveness depends directly on the environmental conditions.

Wobbling Calibration In this case, the CLB is attached to a gyro-gimbal plastic mounting for freely tilt. Additionally, a surface capable of free rotation is required (no metal objects), a magnetic-field-free environment is necessary. The procedure starts by recording data from accelerometers and magnetometers by rotating the CLB in 8 predetermined positions: rotation concerning its 3 orthogonal axes of the CLB, another rotation at 45° concerning the z-axis and their corresponding 4 mirror rotations⁷. A dedicated software uses the collected data to automatically determine the accelerometer and magnetometer offsets (similar to the Plane Calibration) and the necessary rotation matrix

to correct non-linear errors. Data from rotations in the different planes must create an ellipsoid (in the system of coordinates of the magnetometers). The algorithm determines the adjustment to fit the ellipsoid to the sphere shape and determines the offset vector ($\mathbf{A}_{\text{off}}-\mathbf{H}_{\text{off}}$) and matrix corrections ($\mathbf{A}_{\text{rot}}-\mathbf{H}_{\text{rot}}$) needed. In KM3NeT, the default offline calibration starts by taking raw compass data (accelerometers and magnetometers), afterwards, a set of dedicated algorithms estimate the calibration parameters that correspond to the components of the matrix-vector correction needed. In other words, the default calibration technique generates an offset and a matrix correction for each compass accelerometer/magnetometer sensor. Finally, the associated calibration parameters are stored in the DB, defined, for instance, as shown in Equations 3.2-3.3.

$$\mathbf{A}_{\text{offset}} = \begin{pmatrix} 0.0204 \\ -0.0031 \\ 0.0004 \end{pmatrix}; \mathbf{A}_{\text{rot}} = \begin{pmatrix} 0.9929 & -0.0024 & -0.0034 \\ -0.0024 & 1.0094 & -0.0075 \\ -0.0034 & -0.0075 & 0.9978 \end{pmatrix} \quad (3.2)$$

$$\mathbf{H}_{\text{offset}} = \begin{pmatrix} -0.0233 \\ -0.0345 \\ -0.0234 \end{pmatrix}; \mathbf{H}_{\text{rot}} = \begin{pmatrix} 0.9641 & 0.0006 & -0.0026 \\ 0.0006 & 0.9602 & -0.0086 \\ -0.0026 & -0.0086 & 1.0801 \end{pmatrix} \quad (3.3)$$

The implementation process of the offset vector and matrix corrections to raw compass data is explained by means of Equations 3.4-3.5.

$$\text{Accelerometer data (calibrated)} = \mathbf{A}_{\text{cal}} = \mathbf{A}_{\text{rot}} (\mathbf{A} - \mathbf{A}_{\text{off}}) = \begin{pmatrix} A_x \\ A_y \\ A_z \end{pmatrix} \quad (3.4)$$

$$\text{Magnetometer data (calibrated)} = \mathbf{H}_{\text{cal}} = \mathbf{H}_{\text{rot}} (\mathbf{H} - \mathbf{H}_{\text{off}}) = \begin{pmatrix} H_x \\ H_y \\ H_z \end{pmatrix} \quad (3.5)$$

From these latest Equations, the YPR values are reconstructed as:

$$\text{Yaw (Y)} = \text{atan}^2 \left(H_z \sin(R) - H_y \cos(R), H_x \cos(P) + H_y \sin(P) \sin(R) + H_z \sin(P) \cos(R) \right) \quad (3.6)$$

$$\text{Pitch (P)} = \text{atan}^2 \left(A_x, \sqrt{A_y^2 + A_z^2} \right) \quad (3.7)$$

$$\text{Roll (R)} = \text{atan}^2 \left(-A_y, -A_z \right) \quad (3.8)$$

As seen, P and R values are obtained with accelerometer data only while Y depends on both accelerometers and magnetometers data, then Y drags the propagation of their direct related-uncertainties. Once the compass calibration procedure (Plane/Wobbling) has been carried out, two procedures at the KM3NeT labs to guarantee data reliability by the DOM are done: Functionality Test and Acceptance Test. Functionality Test checks the raw measurements of compass do not show values 0 or NaN, and other functional errors in the compass readouts from the DOM (*in-situ*) to the shore station. Acceptance Test verifies the compass data accuracy fulfills KM3NeT performance expectations (*i.e.*, DOM orientation accuracy better than 3.5°) for achieving physics goals. The results are used to know which DOMs are suitable for integration into the corresponding DUs before deployment in the detector sites.

3.2 On-Site operation and Digital Compasses data selection

In the sea environment, the main parameters influencing DOM positioning and orientation are the intensity and direction of the sea current in the detector site. In this sense, the analysis and compass data monitoring developed in this work need to consider different periods to validate the experimental methodology success, thus perform a reliable statistics and systematics studies. Since all the DOMs integrated into each DU are fixed in the same structure, it is possible to infer correlations between DOMs position and their orientation in the same DU, undergoing drag forces and effects of the DU's floating system. The mechanical model stated for KM3NeT DU shape reconstruction considers the drag forces and establishes a relation between the position for all DOMs in the same DU. The orientation of the DOMs in the same DU (same mechanical and environmental conditions) is expected to be correlated, this work proposes the first assessment towards the orientation relations among DOMs along the same DU.

In KM3NeT, the DM is in charge of the data stream communications, from-to DUs (detector site) to-from control room (shore-station). The DataBase (DB) stores ARCA and ORCA data stream at CC-Lyon*, available for offline analysis. The DB stores a permanent record of **A** and **H** data with an associated data structure format. The analysis developed in this work, addresses the data obtained from the DB and the improvement of the software required for a deeper analysis. The compass data are stored in ASCII format in the DB (see Table 3.3) and can be retrieved in a friendly format with the methods already developed by the DM maintainers (software libraries). The default access to the DB and data retrieving (Python-based codes) is developed and maintained by the KM3NeT Collaboration Software and Computing Group.

Name	Data Type	Meaning
DETID	int	Identifier number associated to a given detector.
RUN	int	Run number associated with a data collection period.
UNIXTIME	int	Timestamp according Unix system format, describe a specific point of time.
DUID	int	Identifier number for a specified DU of the detectors.
FLOORID	int	Floor where a DOM in each DU is located.
CLBUPI	string	CLB Unique Product Identifier (CLB code name for DB indication).
AHRS_A	float	Accelerometer, data of each axis board is stored independently, the (x,y,z) axes, corresponding to AHRS_A0, AHRS_A1, AHRS_A2, respectively.
AHRS_H	float	Magnetometers, data of each axis board is stored independently, the (x,y,z) axes, corresponding to AHRS_H0, AHRS_H1, AHRS_H2, respectively.

Table 3.3: Compass Data format in the KM3NeT DB. The already developed methods to retrieve compass data can query an specific dataset using these parameters.

*[https : //cc.in2p3.fr/](https://cc.in2p3.fr/)

The Figure 3.1 shows a specific extract of compass data retrieved for ORCA6 DU1F9 compass (RUN 8501). Additionally, each electronic component integrated into the detector site has a Unique Product Identifier (UPI) label. In the DB, compass data are linked to the CLB's UPI in which the compass is installed.

	RUN	UNIXTIME	DUID	FLOORID	CLBUPI	AHRS_A0	AHRS_A1	AHRS_A2	AHRS_H0	AHRS_H1	AHRS_H2
0	8501	1597838400477	9	1	3.4.3.2/V2-2-1/2.284	-0.008	0.014	1.040	-0.086667	0.058182	-0.199697
107	8501	1597838410477	9	1	3.4.3.2/V2-2-1/2.284	-0.008	0.014	1.041	-0.089091	0.059394	-0.199091
216	8501	1597838420477	9	1	3.4.3.2/V2-2-1/2.284	-0.008	0.014	1.041	-0.090000	0.057879	-0.200000
325	8501	1597838430484	9	1	3.4.3.2/V2-2-1/2.284	-0.008	0.014	1.041	-0.086667	0.059394	-0.201515
432	8501	1597838440477	9	1	3.4.3.2/V2-2-1/2.284	-0.008	0.014	1.041	-0.087273	0.058182	-0.199697

Figure 3.1: Extract of compass data from the DB, labeled in the DB query.

3.2.1 Data filtering

The data selection considerations constitutes an important basis of this work, hence, next formalisms are of consideration:

1. **Calibration version.** Performance of the available calibration procedures affects the compass data accuracy.
 - **Calibration v1.** Defines the absence of calibration parameters for a certain compass.
 - **Calibration v2.** Defines the implementation of Plane Calibration⁶.
 - **Calibration v3.** Defines the implementation of Wobbling Calibration⁷.
2. **Instrumental aspects.** Some situations along the detector construction/operation impact compasses performance.
 - **No Operational.** Compass data not recorded (DOM is switch-off).
3. **Compass Firmware.** Firmware versions installed in the compass board are directly related with the DOM performance.
 - **FW v4.1.** For AHRS-LNS compasses installed with firmware v4.1, expected behavior in compasses data stream is observed.
 - **FW <4.1.** For AHRS-LNS compasses installed with firmware < v4.1, atypical behavior is observed in the data stream.
 - **No FW.** For LSM303 compasses, it does not need firmware.
4. **Compass Data default filtering.** For compasses, data filtering is done to guarantee data quality.
 - (a) Exclude data if any of components of **A-H** vector (Equation 3.1) reaches zero by calibration parameters implementation.
 - (b) Exclude data if any of components of **A-H** vector is zero.
 - (c) Cleaning duplicates. Data is removed if any of **A-H** vector components is the same in consecutive measurements.

5. **Sea current period.** According to the selected period, different environmental conditions induce DOMs translation/rotation movements. This work considers two data periods:

- **Short-Period.** Around 15 days of data, weak contributions from sea current to the DOM orientation are expected, this is used to determine the expected behavior of compasses in "optimal conditions".
- **Long-Period.** Around 9 months of data, considers all possible variations of intensity and direction of the sea current on the compass data.

In ORCA6, DU11 contains the LSM303 model, except F15, while in the rest of DUs, the AHRS-LNS model is implemented. Figure 3.2 shows the kind of duplicated (random) data obtained for AHRS-LNS and LSM303 compass model, implemented in DU10 and DU11.

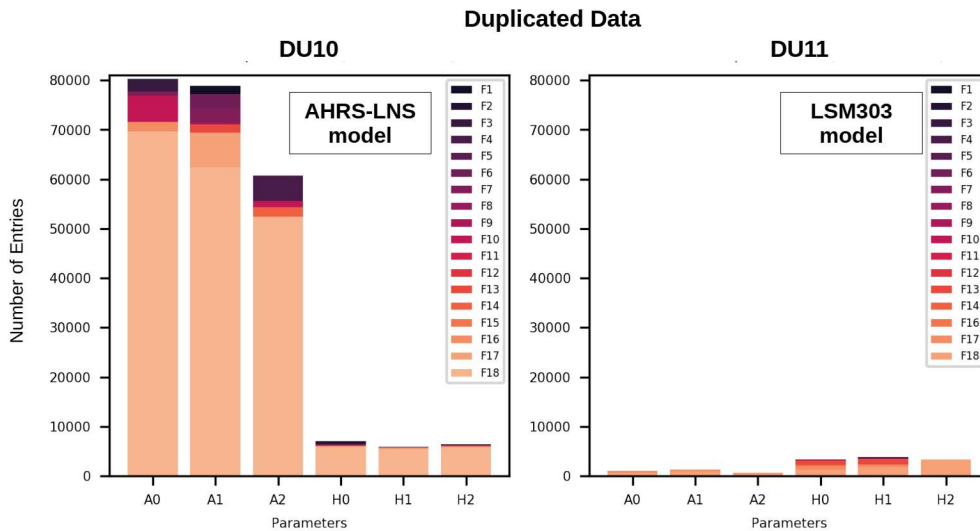


Figure 3.2: A sample of duplicated data in ORCA6 compasses (RUN 8501-8550). AHRS-LNS accelerometers representatively shows a greater number of duplicates.

As seen, the number of duplicated entries is representatively larger in the **A** components for AHRS-LNS model, what is also identified for other DUs, independently of the analyzed period. For the LSM303 model, the duplicated data is significantly lesser than the number of duplicates found in the AHRS-LNS readouts. Default filtering conditions remove an entry if at least one **A-H** component is identified as a duplicate, as represented in Figure 3.3 (the duplicates identified in the same **A** component are surrounded by colored boxes). Preliminarily, it is observed that the duplicates can appear randomly, what may contradict the idea that duplicates arise from instrumental problems, and therefore should affect all **A-H** components at once.

	UNIXTIME	CLBUPI	RUN	AHRS_A0	AHRS_A1	AHRS_A2	AHRS_H0	AHRS_H1	AHRS_H2
172	1.5800467308560e+09	3.4.3.2/V2-2-1/2.132	7221	-1.0110000371933	-0.0490000024438	0.0230000019073	0.1869696974754	-0.1248484849930	-0.0312121212482
360	1.5800468409060e+09	3.4.3.2/V2-2-1/2.132	7221	-1.0110000371933	-0.0500000007451	0.0230000019073	0.1845454573631	-0.1254545450211	-0.0293939393014
378	1.5800468508560e+09	3.4.3.2/V2-2-1/2.132	7221	-1.0110000371933	-0.0500000007451	0.0230000019073	0.1863636374474	-0.1245454549789	-0.0312121212482
395	1.5800468608560e+09	3.4.3.2/V2-2-1/2.132	7221	-1.0110000371933	-0.0500000007451	0.0230000019073	0.1881818175316	-0.1266666650772	-0.0287878792733
411	1.5800468708580e+09	3.4.3.2/V2-2-1/2.132	7221	-1.0110000371933	-0.0500000007451	0.0230000019073	0.1878787875175	-0.1236363649368	-0.0309090912342
429	1.5800468808630e+09	3.4.3.2/V2-2-1/2.132	7221	-1.0110000371933	-0.0500000007451	0.0230000019073	0.1878787875175	-0.1257575750351	-0.0299999993294
446	1.5800468908560e+09	3.4.3.2/V2-2-1/2.132	7221	-1.0110000371933	-0.0500000007451	-0.0240000002086	0.1866666674614	-0.1284848451614	-0.0303030312061
462	1.5800469008560e+09	3.4.3.2/V2-2-1/2.132	7221	-1.0110000371933	-0.0500000007451	-0.0240000002086	0.1896969676018	-0.1284848451614	-0.0290909092873
479	1.5800469108560e+09	3.4.3.2/V2-2-1/2.132	7221	-1.0110000371933	-0.0490000024438	-0.0230000019073	0.1884848475456	-0.1233333349228	-0.0312121212482
495	1.5800469208600e+09	3.4.3.2/V2-2-1/2.132	7221	-1.0110000371933	-0.0490000024438	-0.0240000002086	0.1857575774193	-0.1257575750351	-0.0321212112904
512	1.5800469308600e+09	3.4.3.2/V2-2-1/2.132	7221	-1.0110000371933	-0.0500000007451	0.0230000019073	0.1875757575035	-0.1266666650772	-0.0303030312061
697	1.5800470408590e+09	3.4.3.2/V2-2-1/2.132	7222	-1.0110000371933	-0.0490000024438	0.0230000019073	0.1878787875175	-0.1245454549789	-0.0321212112904
711	1.5800470508610e+09	3.4.3.2/V2-2-1/2.132	7222	-1.0110000371933	-0.0490000024438	0.0230000019073	0.1869696974754	-0.1257575750351	-0.0321212112904
729	1.5800470608560e+09	3.4.3.2/V2-2-1/2.132	7222	-1.0110000371933	-0.0500000007451	0.0230000019073	0.1872727274895	-0.1263636350632	-0.0309090912342
745	1.5800470708610e+09	3.4.3.2/V2-2-1/2.132	7222	-1.0110000371933	-0.0500000007451	-0.0230000019073	0.1866666674614	-0.1290909051895	-0.0287878792733

Figure 3.3: Duplicated entries from a fragment of accelerometer data. A particular case is identified for ORCA6 DU3-F4 (AHRS-LNS model), RUN 7221-7222. Colored boxes enclose the "duplicates" found in different columns.

Two main effects associated to compass data retrieved from DB are hence identified:

- **Resolution Effect.** The sensitivity of the AHRS-LNS accelerometer allows a measurement limit of 3 significant decimal places, the situation is not the same for the accelerometers of the LSM303 model. The existence of a representative number of duplicates in AHRS-LNS accelerometers can be related to the accelerometer board sensitivity. The resolution effect is also associated with the fact that accelerometers and magnetometers in the AHRS-LNS constitute separated sensor chips implemented on the same compass board, showing different data sensitivity/resolution. This work proposes improved data filtering conditions for both Digital Compasses models.
- **Communication Effect.** The compasses data show the presence of Non-Associated-Numbers (NaN) in the dataset retrieved from the DB. The NaN found in a compass entry interferes with the default filtering algorithms that identify duplicates. It has been corrected in this work with a simple routine discarding NaN entries.

The structure of the unfiltered compass data handling technique developed in this work is represented in Figure 3.4, each column represents a **A** or **H** component, and each row corresponds to a compass measurement at a given time.

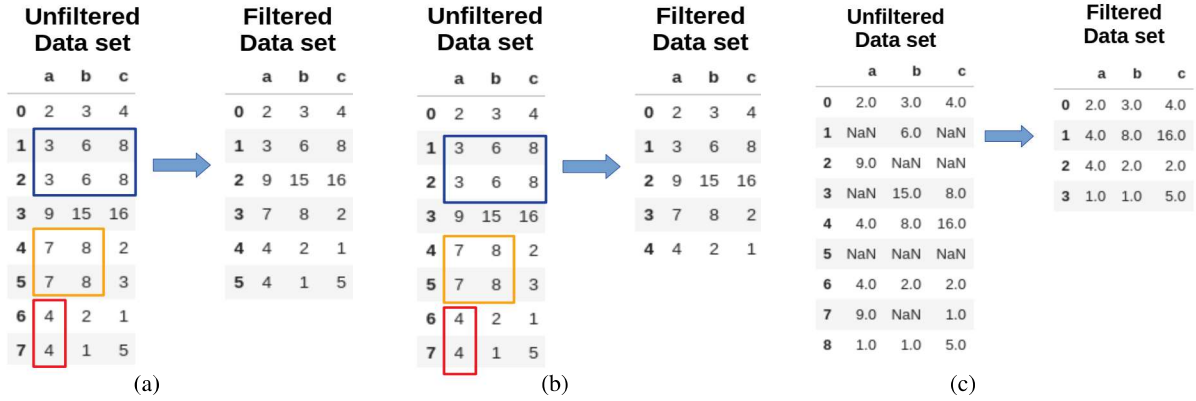


Figure 3.4: Duplicates filtering technique for compass data according to Resolution and Communication Effect applied over three different cases (a,b,c).

The algorithm identifies duplicates comparing row-by-row the values of each **A** or **H** component in the datasets. According to the Resolution and Communication Effect considerations, for AHRS-LNS **A**, only the data with at least two column values identified as duplicates are filtered (data surrounded by blue/yellow rectangle). For the AHRS-LNS **H** and LSM303 **A-H** data, if at least one column value is identified as duplicate, the row is discarded (data surrounded by rectangles). A row in the unfiltered dataset is discarded if it contains NaN in its columns. The default filtering conditions are thus "upgraded" to the **Improve data filtering**, as an important contribution of this work, summarized by Table 3.4, in order-wise implementation.

Improved Data Filtering Conditions

1. Exclude data if any of components of **A-H** reach zero by calibration parameters implementation.
 2. Exclude data if any of components of **A-H** is zero.
 3. Eliminate rows with NaN values.
 4. Cleaning duplicates in **A-H** in consecutive measurements:
 - 4.1 For AHRS-LNS (**A** data only): data are discarded if at least two parameter of **A** are identified as duplicates.
 - 4.2 For AHRS-LNS (**H** data only) and LSM303 data: data is discarded if at least one parameter (components of **A-H**) is identified as duplicate.
-

Table 3.4: Improved data filtering conditions for compass data developed in this work.

In this work, only compass data from ORCA6 were considered. The number of integrated compasses reaches 108 in 6 DUs, with some key factors for data selection summarized in Figure 3.5.

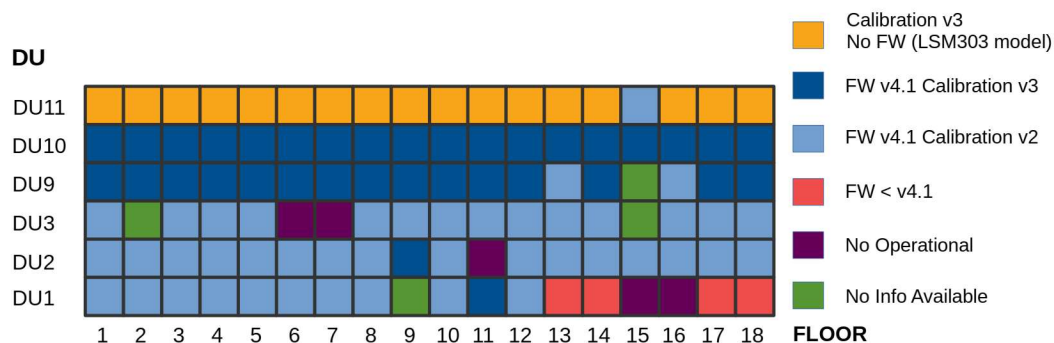


Figure 3.5: Some key factors (Calibration, firmware versions) for compasses in ORCA6 regarding data selection in this work.

Looking to analyze the sea current influence on the DOM orientation, two periods for ORCA6 were selected.

- **Short-Period:** RUN 8000 - 8085 (2020/05/12 - 2020/05/30).
- **Long-Period:** RUN 7221 - 8721 (2020/01/26 - 2020/10/05).

By considering the improved data filtering conditions applied to ORCA6 with the best calibration and firmware versions, for the Short and Long-Period, Table 3.5 summarises the consolidated criteria for compass data selection.

Consolidated data selection criteria for compasses (ORCA6)		
Criteria	Compass Requirements	Comments
1. Firmware Version	4.1	AHRS-LNS needs to be FW 4.1. For LSM303, no FW is needed.
2. Calibration Version	v2, v3	Compasses with suitable XML calibration files at DB.
3. Data Filter	Improved filtering	As defined in Table 3.4.
4. Time Period	<ul style="list-style-type: none"> • Short-Period (RUN 8000 – 8085) • Long-Period (RUN 7221 – 8721) 	Two periods accounting for global effects of the sea current. Short: no significant orientation changes are expected, Long: representative changes are expected.

Table 3.5: Consolidated data selection criteria (cuts/filtering) for compasses data, meaning unbiased inputs towards reasonable systematics study.

3.3 Digital Compasses performance and systematics

The preliminary analysis (method) of uncertainties (systematics study) in compasses for the consolidated data selection in ORCA6 is presented in this section. The first part of the analysis consists of handling the instrumental effects that may not have been totally suppressed during the offline calibration (Plane/Wobbling). These effects (indirect) become propagated when using the YPR equations, impacting the correct reconstruction of the magnitudes (direct effects from $|\mathbf{A}|$ - $|\mathbf{H}|$ readouts included). Figure 3.6 summarizes possible sources of uncertainty related to the YPR calculation.

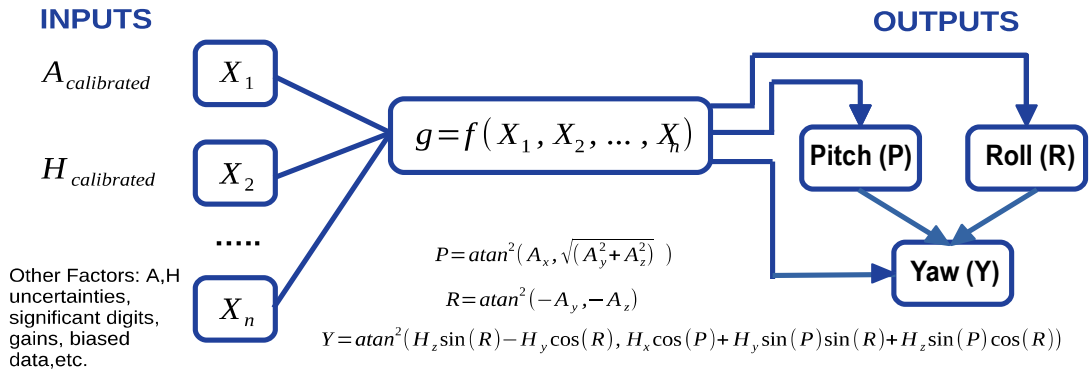


Figure 3.6: General scheme for \mathbf{A} - \mathbf{H} data and uncertainty factors in YPR calculation. The proposed model to reconstruct the YPR values indicates the Y values contain the propagation of the global effects (indirect, direct) of systematic uncertainties.

According to Figure 3.6, the global effect of the different uncertainty sources goes through YPR equations impacting the orientation values. The uncertainties associated with P and R are propagated to Y, which keeps the effects of the direct uncertainties coming from \mathbf{A} and \mathbf{H} . On the other hand, P and R keep the effects of uncertainty propagated by \mathbf{A} only as observed. Since YPR equations are known, a method of propagating uncertainties using partial derivatives may sound reasonable to determine the magnitude of the global uncertainty effects on the calculated orientation data. However, there is no additional information beyond the compass data recovered from the DB in this work. Preliminary, it has been found that residual uncertainties are different for each compass. Some effects associated with each compass can be partially canceled in the ratios of the YPR equations and the magnitude of the propagated uncertainty linked to sign interpretations (compensation direction), hence, partial derivatives may not be trustworthy enough. Propagation equations at higher orders are needed, implying covariance effects between P and R concerning Y. Given the restriction established for the error propagation methods already commented, this work formally proposes a model to work around the residual uncertainties associated with each compass differently.

3.3.1 The Accelerometer and Magnetometer modulus

The compass board housing the accelerometer and magnetometer sensors estimate the total acceleration vector and the local magnetic field in the surroundings, respectively. The modulus of accelerometer components in vector form (Equation 3.4) needs to be equivalent to the total acceleration vector modulus. Similarly, the modulus of magnetometers components in vector form (Equation 3.5) needs to be equivalent to the modulus of the local magnetic field⁶. The total acceleration vector and the local magnetic field modulus are assumed stable quantities with slight variations over time that can be ignored.

- **Total acceleration vector (\vec{A})**. The modulus of this vector estimates Earth's gravity ($\sim 9.8 \text{ m/s}^2$), the direction of the vector is perpendicular to the Earth's surface plane (Figure 3.7a). Each compass accelerometer in vector form estimates a projection of the total acceleration vector in each of its 3 orthogonal axes. Then, the accelerometer components vector modulus is equivalent to the total acceleration vector modulus (Figure 3.7b), regardless of the orientation of the compass board or reference frame.

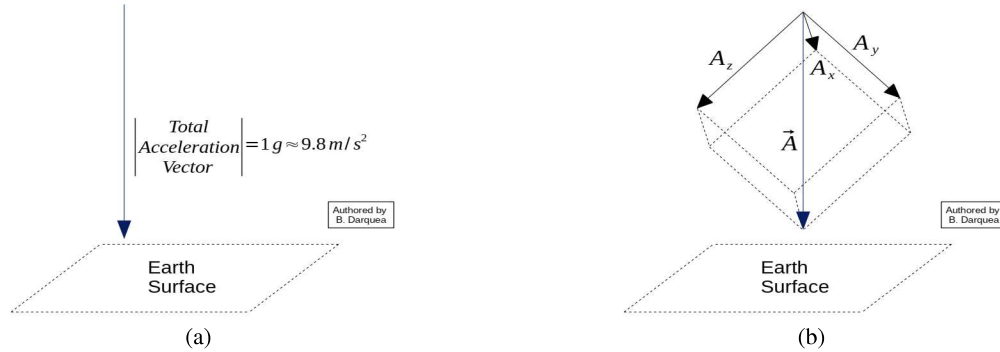


Figure 3.7: Acceleration vectors in the global reference system. (a) Acceleration vector in Earth's reference frame. (b) Acceleration vector estimated by compass board (accelerometer).

- **Local magnetic field vector (\vec{H})**. The Earth's magnetic field vector modulus $|\vec{B}|$ (Figure 3.8a) along with minor magnetic contributions are estimated by magnetometer components vector modulus $|\vec{H}|$ (Figure 3.8b). Then, each magnetometer's orthogonal axes within the compass board are projections of local magnetic field vector axes (Earth and local magnetic contributions). The specific value for $|\vec{B}|$ depends on the longitude, latitude, and height of the terrestrial position (ORCA6 detector site is used).

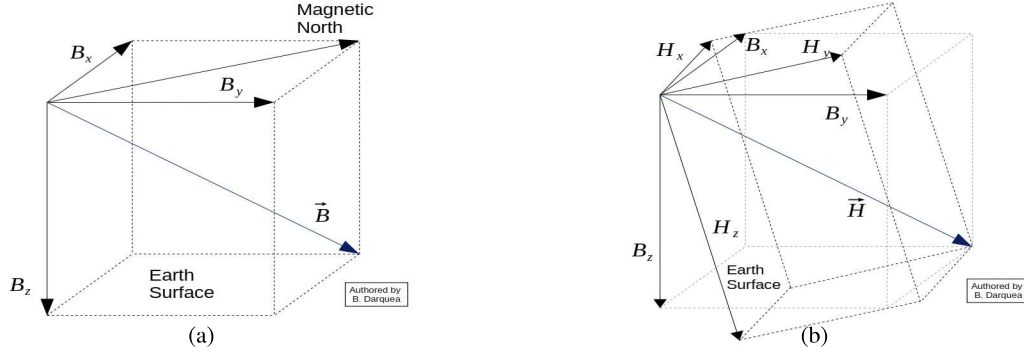


Figure 3.8: Magnetic vectors in the global reference system. (a) Earth's magnetic field vector. (b) Magnetic field vector estimated by compass board (magnetometer).

The accelerometer and magnetometer vector modulus are defined in Equation 3.9.

$$|\vec{A}| = \sqrt{A_x^2 + A_y^2 + A_z^2} \quad ; \quad |\vec{H}| = \sqrt{H_x^2 + H_y^2 + H_z^2} \quad (3.9)$$

In the KM3NeT compasses, accelerometer readouts are scaled, precisely, as a function of g ($g \simeq 9.8 \text{ m/s}^2$ Earth's gravity), so $|\vec{A}|$ has to be equivalent to $1g$. In the case of the magnetometers, $|\vec{H}|$ has to be equivalent to $|\vec{B}|$ plus other "local" magnetic contributions. The location of $|\vec{B}|$ for the ORCA6 detector site (4248' N 0602' E, depth 2450 m, 40 km offshore from Toulon, France) points 0.465 gauss in the surroundings, according to World Magnetic Model[†]. The estimated value for $|\vec{B}|$ (for the proposed analysis) needs to be equivalent to $|\vec{H}|$ value. With this idea, the accelerometer/magnetometer module technique for inspection on compass uncertainties are based on comparing how well $|\vec{A}|$ and $|\vec{H}|$ (from compass data) estimate the total acceleration and local magnetic field modulus, respectively. In principle, the more representative the difference to the modulus, the larger the uncertainty propagated over the compass data.

[†]Taken from National Centers for Environmental Information at <https://www.ngdc.noaa.gov>

Chapter 4

Results and Discussion

In this chapter, offline data monitoring considerations are developed from the sanity checks over compass data retrieved, along with the evaluation of the frequency and distribution over time of recorded events. Besides, in this chapter, a parameterization is proposed for assessment of systematics (a first attempt) for ORCA6 compasses. Additionally, the results of parallel works that emerged in the development of this work are also presented.

4.1 Compass data, monitoring and orientation

As commented in previous chapters, DB stores a permanent record of compass data streamed to the KM3NeT servers, coming from its accelerometer or magnetometers. The offline compass data analysis is carried out by retrieving the DB compass data for a certain detector period, calculating the corresponding YPR orientation values, the online monitoring cannot directly verify the DB-related issues. Final sanity checks for consolidated data selection follows:

- **Frequency of recorded events.** It verifies that the DM frequency programmed for the compass data recording is the same as the one observed in the compass dataset retrieved from the DB. An effective way to calculate the frequency associated with the dataset is done by comparing and evaluating the time differences of two consecutive measurements from the compass dataset, using the recorded times (UNIXTIME format) converted to Coordinated Universal Time (UTC). Figure 4.1a shows the estimated time differences for each of the ORCA6 DU1 Floors. The estimated time differences distribution points out the frequency (time difference histogram) is around 1 compass event recorded every 10 seconds. Currently, the DM recording frequency is set to 10 seconds. In this example, the recording frequency estimated from the compass dataset retrieved from the DB is similar to the value stated by the DM. Similar results are obtained for an arbitrary compass dataset (Figure A.1).
- **Compasses communication.** The distribution over time of the compass measurements is also an indicator of the communication sanity. Some interruptions in the compass data stream are expected, as Figure 4.1b shows. As an example, F15 and F16 show no data records for the entire period, it is usually reported (black

color) rarely during detectors operation*. Similar results are obtained if it looks for a random compass dataset (Figure A.2).

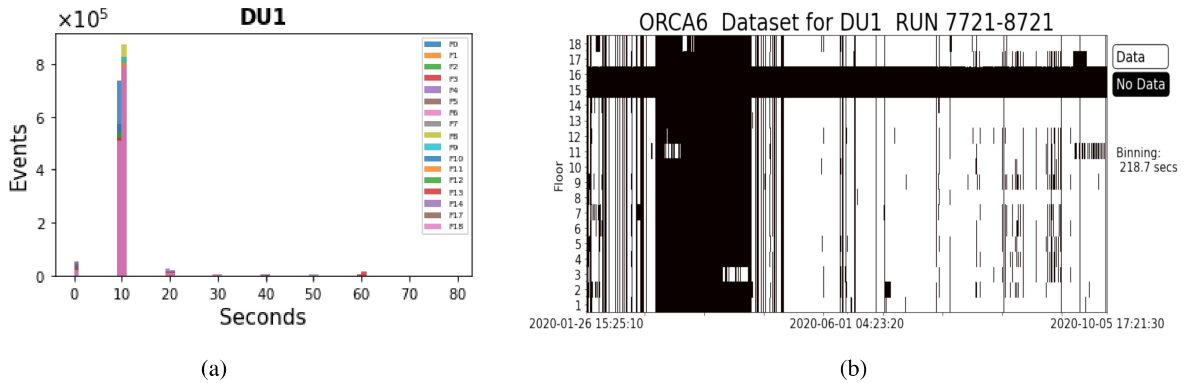


Figure 4.1: Frequency of recorded events for compass data. (a) Recording frequency histogram. (b) Distribution of compass readout over time.

By applying our consolidated data selection (Table 3.5), YPR orientation values are reconstructed from accelerometer and magnetometer data, in agreement to Equations 3.6-3.8. In this sense, Figures 4.2-4.4 show P, R and Y reconstructed values. It is observed that all YPR orientation values behave differently over time, result of the size of the orientation changes. For instance, the range of Y values is broader than the range of PR values. This difference can be explained because each DOM is fixed vertically in the DU. The rotations tend to have less restrictions around the z-axis (Y parameter) than rotations in the horizontal plane (PR). The Short-Period (2020/05/12-2020/05/30) shows minimal variations as expected and the Long-Period (2020/01/26 - 2020/10/05) evidences non-periodic variations in orientation, however, an average angle is clearly constrained. In both periods, a very marked trend to conserve Y orientation is thus observed. The same reasoning is valid for PR. It represents a "nominal" orientation for each compass available in each DU of the ORCA6 detector. This nominal orientation represents the averaged of the corresponding orientation values. The size of the orientation changes observed in the Long-Period is mainly associated with external factors impacting the orientation of the DOMs, namely the global effect of sea current observables (intensity, direction), mainly impacting Y. In the Short-Period, the sea current is minimal, thus the orientations changes are minimal.

*<https://elog.km3net.de/Operations+FR/3592>

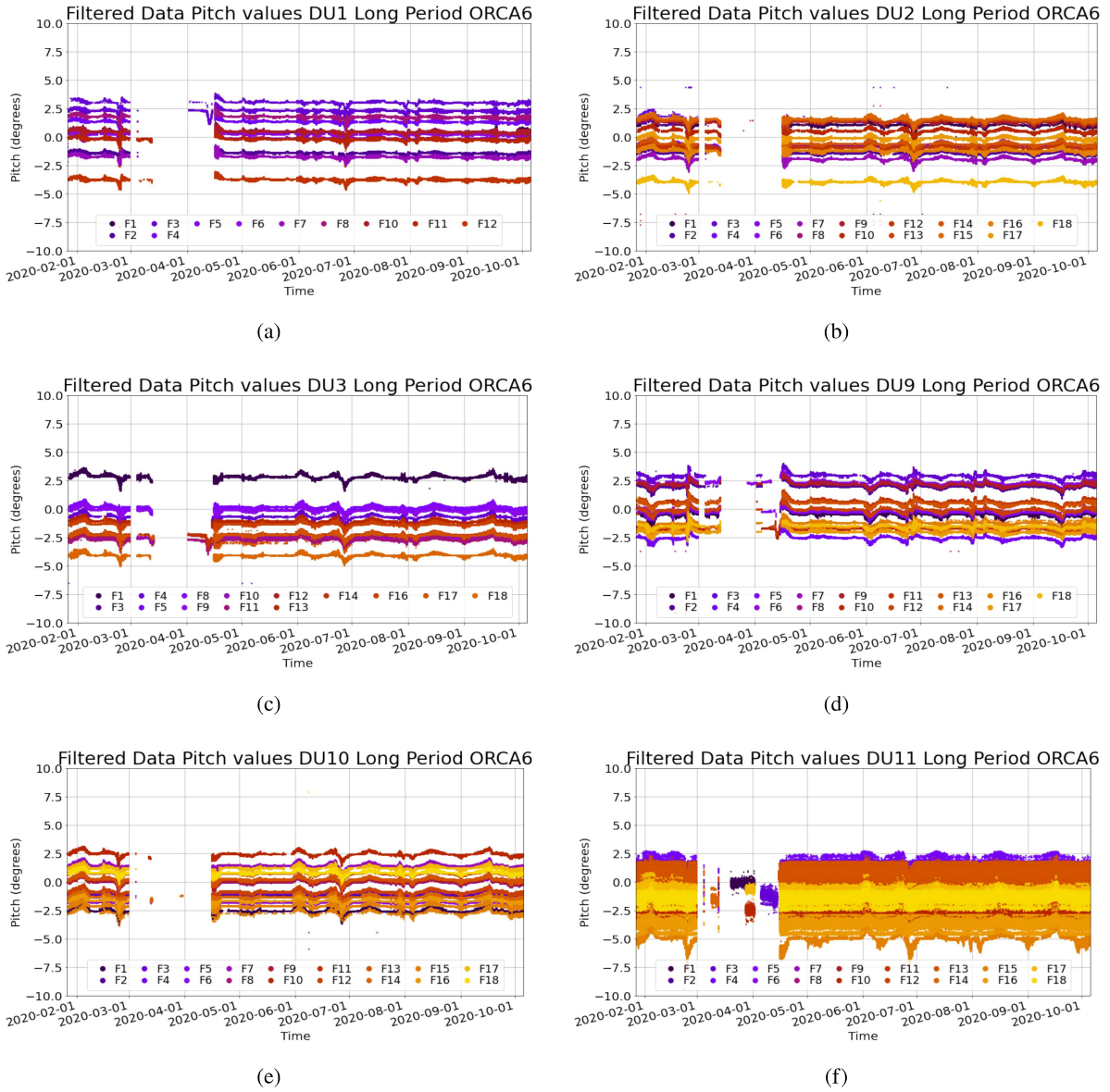


Figure 4.2: Reconstructed Pitch (P) values for ORCA6 compasses in Long-Period (includes the Short-Period). Each color represents compass readouts along the DU. Time format: yyyy-mm-dd.

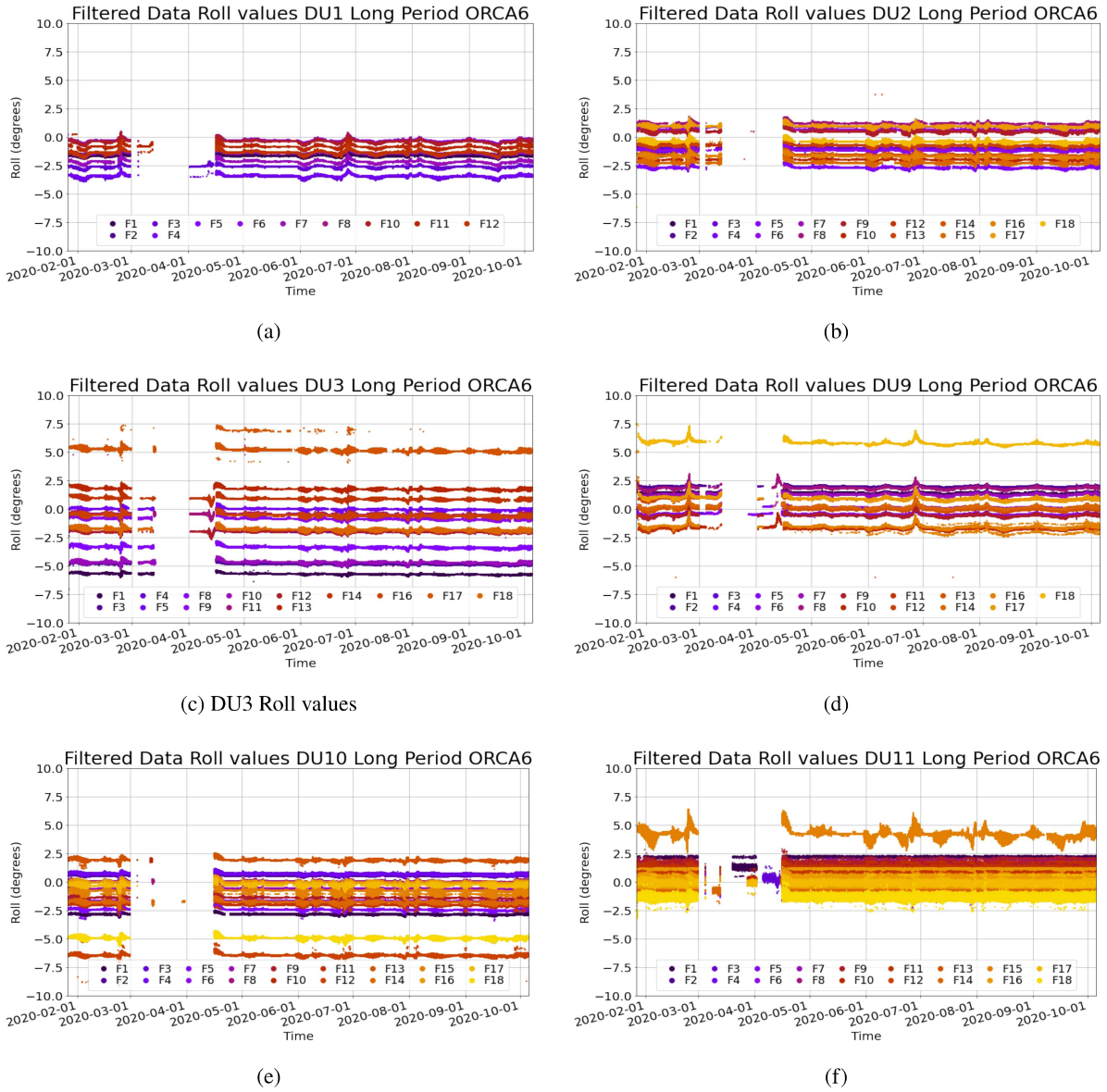


Figure 4.3: Reconstructed Roll (R) values for ORCA6 compasses in Long-Period (includes the Short-Period). Each color represents compass readouts along the DU. Time format: yyyy-mm-dd.



Figure 4.4: Reconstructed Yaw (Y) values for ORCA6 compasses in Long-Period (includes Short-Period). Each color represents compass readouts along the DU. Time format: yyyy-mm-dd.

4.2 Compass systematics

The values of $|\vec{A}|$ and $|\vec{H}|$ are expected don't be changing over time, regardless of the orientation/position of the compass board, they estimate the total acceleration and Earth's magnetic vector modulus, respectively. In this sense, the effect of uncertainties not totally suppressed by calibration would also be conserved in time. Hence, the uncertainties over each compass can be estimated by comparing how $|\vec{A}|$ and $|\vec{H}|$ differ with respect to the reference values ($|\vec{A}| = 1\text{ g}$ and $|\vec{H}| \approx 0.465\text{ gauss}$). As seen in Figures 4.5 and 4.6, $|\vec{A}|$ and $|\vec{H}|$ readouts associated to the same compass model are consistent, nonetheless, "spurious values" are also present mainly for $|\vec{H}|$ data, presumable because external factors. In Figure 4.5a for AHRS-LNS data from DU9, the readouts seem to be very close to the reference $|\vec{A}| = 1\text{ g}$. In Figure 4.5b for LSM303 data from DU11, the data range is wider.

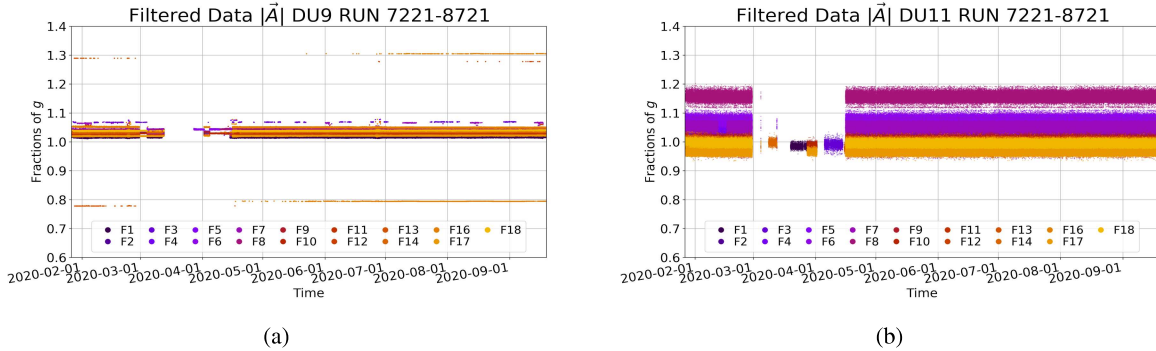


Figure 4.5: Acceleration vector modulus $|\vec{A}|$ estimated by both compass models in ORCA6 Long-Period (except F15). (a) $|\vec{A}|$ values for AHRS-LNS in DU9. (b) $|\vec{A}|$ values for LSM303 in DU11.

In Figure 4.6a, the data is clustered around the reference $|\vec{H}| = 0.465\text{ gauss}$, but it is not clear enough for LSM303 compasses (DU11), as Figure 4.6b represents. The distribution of $|\vec{H}|$ values is stable over time than LSM303 values, however, data range is representatively wider.

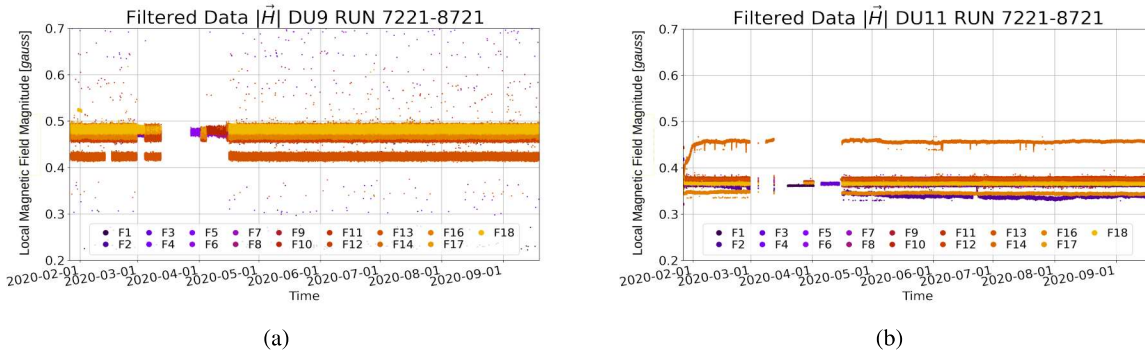


Figure 4.6: Magnetic vector modulus $|\vec{H}|$ estimated by both compass model in ORCA6 Long-Period (except F15). (a) $|\vec{H}|$ values for AHRS-LNS in DU9. (b) $|\vec{H}|$ values for LSM303 in DU11.

On the other hand, Figure 4.7 and 4.8 show "heat maps" for $|\vec{A}|$ and $|\vec{H}|$ averaged values for joint operation of ORCA6 compasses. Figure 4.7a supports the AHRS-LNS (DU 1, 2, 3, 9, 10 and DU 11 F15) and LSM303 (DU11 except F15) readouts are, nonetheless, statistically compatible (close tonality), except for DU11 F8 and F15. Figure 4.7b, endorse this observation: the mean values of $|\vec{A}|$ are very close (except for DU11 F8), where the reference is represented as an horizontal purple line ($|\vec{A}| = 1 g$).

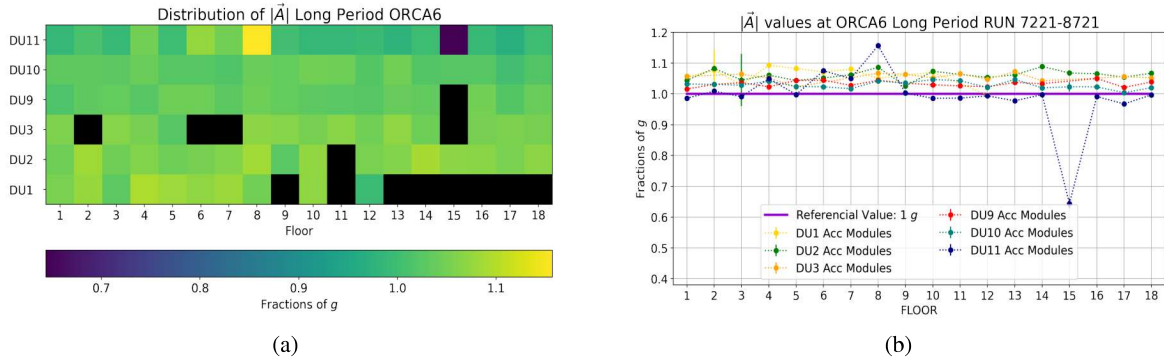


Figure 4.7: $|\vec{A}|$ averaged values overtime for ORCA6 compasses (Long-Period). (a) Heat map: fractions of g by DU and Floor of all DUs (unavailable compasses in black). (b) Fractions of g by Floor and reference value ($|\vec{A}| = 1 g$) for DUs detailed comparison.

As done for $|\vec{A}|$, Figure 4.8a shows that $|\vec{H}|$ mean values roughly estimate the reference for AHRS-LNS model (DU1,2,3,9,10 and DU11F15), except for DU3F17. Most of LSM303 compasses (DU11 except F15) show different values with respect to the AHRS-LNS model, what is supported by results in Figure 4.8b. $|\vec{H}|$ mean values for DU11 are far from reference (violet line $|\vec{H}| = 0.465 gauss$), except DU11 F14-15. Previous analysis in KM3NeT showed that the $|\vec{H}|$ estimated from AHRS-LNS calibrated data required a 2.04 scale factor correction so that the calculated modulus adequately estimates the local magnetic vector modulus[†]. For the LSM303 model, a scale factor is not considered yet.

[†]Scale Factor for AHRS-LNS magnetometers obtained experimentally by KM3NeT researchers.

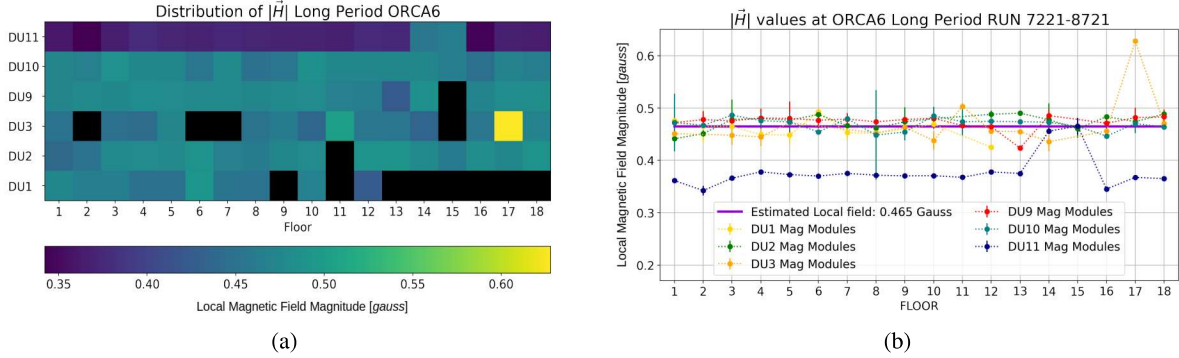


Figure 4.8: $|\vec{H}|$ averaged values overtime for ORCA6 compasses (Long-Period). (a) Heat map, gauss by DU and Floor of all DUs (unavailable compasses appear in black color). (b) Gauss by Floor and reference value ($|\vec{H}| = 0.465$ gauss) comparison.

All indicates that ORCA6 compasses are mostly correctly calibrated (the estimated modulus adequately represents the reference for $|\vec{A}|$ and $|\vec{H}|$), with few exceptions. Regardless the size, the differences may represent the most representative uncertainties for compass data. Table A.1 lists $|\vec{A}|$ and $|\vec{H}|$ mean values (\bar{X}), standard deviation (SD) and percentage change with respect to the reference in the Long-Period. In general, Table A.1 shows that $|\vec{A}|$ and $|\vec{H}|$ mean values do not have strong variations over time. The standard deviation of $|\vec{A}|$ is between [0.001 - 0.07] fractions of g , the standard deviation of $|\vec{H}|$ is between [0.001 - 0.06] gauss, using more than 1.5×10^9 samples contained in the Long-Period. The variation of $|\vec{A}|$ is between [0.19 - 7.51] % with respect to the reference considering the compasses of all DUs, in exceptional cases reaching [15.7 - 35.62] % (*i.e.* DU11 F8 and F15). For AHRS-LNS $|\vec{H}|$ variation is between [0.01 - 8.89] %, one exceptional case with 35.62% (DU11F15) for LSM303 model in DU11 (all Floors except F15). The variation of $|\vec{H}|$ is between [1.96-26.4] % with respect to the reference, the largest variation in the LSM303 do not necessarily indicate miscalibration of the LSM303 model, but a scale factor may be needed for estimate correctly the reference. Considering the results obtained in Table A.1, it is possible to estimate how much YPR values change with respect to $|\vec{A}|$ and $|\vec{H}|$ (next section).

4.2.1 Compass modulus (accelerometer, magnetometer) and YPR orientation values

In Figure 4.9 a different representation for Y in DU11 is shown, being possible to appreciate the spread of this magnitude along the DU having the number of events as indicator. From Figure 4.9a (Short-Period), Y values from F1-18 show appreciable differences, but considering changes between nearby floors only (*i.e.* F1 and F2) similar orientations are obtained. In general, compasses integrated into the same DU undergo to similar mechanical and environmental conditions. The spread in Y along the DU can be associated to the influence of unidirectional sea currents, affecting DOM orientation, or, generated by the propagation of uncertainties over Y estimated. Over Figure 4.9b (Long-Period), the differences between nearby Floors become statistically compatible with the Short-Period data. Regardless of the period, external factors (sea current intensity, direction) are not impacting Y readout

significantly, thus an indicator of robustness of the experimental methodology.

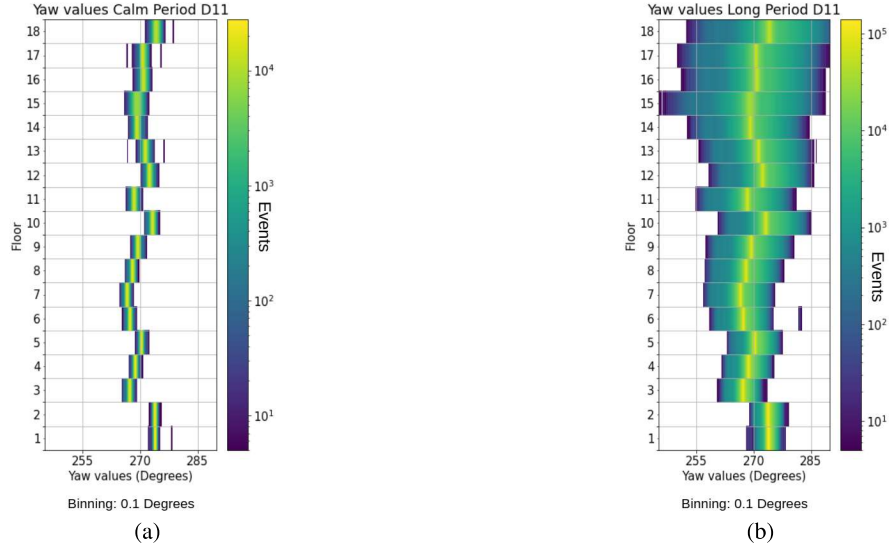


Figure 4.9: 2D orientation distribution of Y (consolidated data selection). (a) Short (Calm) Period dataset. (b) Long-Period dataset.

Back to $|\vec{A}|$ and $|\vec{H}|$, the existence of special cases should be related (in principle) with identifiable differences in the estimated orientation from those compasses data, i.e., looking at $|\vec{A}|$ and $|\vec{H}|$ variation from the reference and compare with the orientation distribution. The comparison of $|\vec{A}|$ and $|\vec{H}|$ modulus, with the 2D orientation distribution of Y in Short-Period is shown in Figure 4.10. As seen for DU1, $|\vec{A}|$ and $|\vec{H}|$ variations from their reference are between [0.38-9.33]% and [0.85-8.57]% respectively. For DU2, $|\vec{A}|$ and $|\vec{H}|$ variations are between [2.56-8.63]% and [0.25-5.41]% respectively. DU3F17 represents a particular case of DU3 where $|\vec{H}|$ variation is about 35.05% from the reference value, while $|\vec{A}|$ variation is about 5.63%. DU9-D10 are identified with the best performance in $|\vec{A}|$ and $|\vec{H}|$ estimations. DU11 $|\vec{A}|$ variation is between [1.96-26.4]%. As concluded by visual inspection, the assumption that $|\vec{A}|$ and $|\vec{H}|$ variation may estimate uncertainties for $\mathbf{A-H}$ is not sufficient to determine a global effect over YPR orientations. It seems that representative shifts in Y between nearby Floors is not directly related with the percentage change estimated for $|\vec{A}|$ and $|\vec{H}|$. Considering the $|\vec{A}|$ and $|\vec{H}|$ forms in Equations 3.1, their components are squared, then losing the sign (direction) of associated uncertainties, so, variations (Table A.1) may maximize/minimize the estimations. Thus, in general, significant variation of vector modulus doesn't suggest a significant shifts in Y.

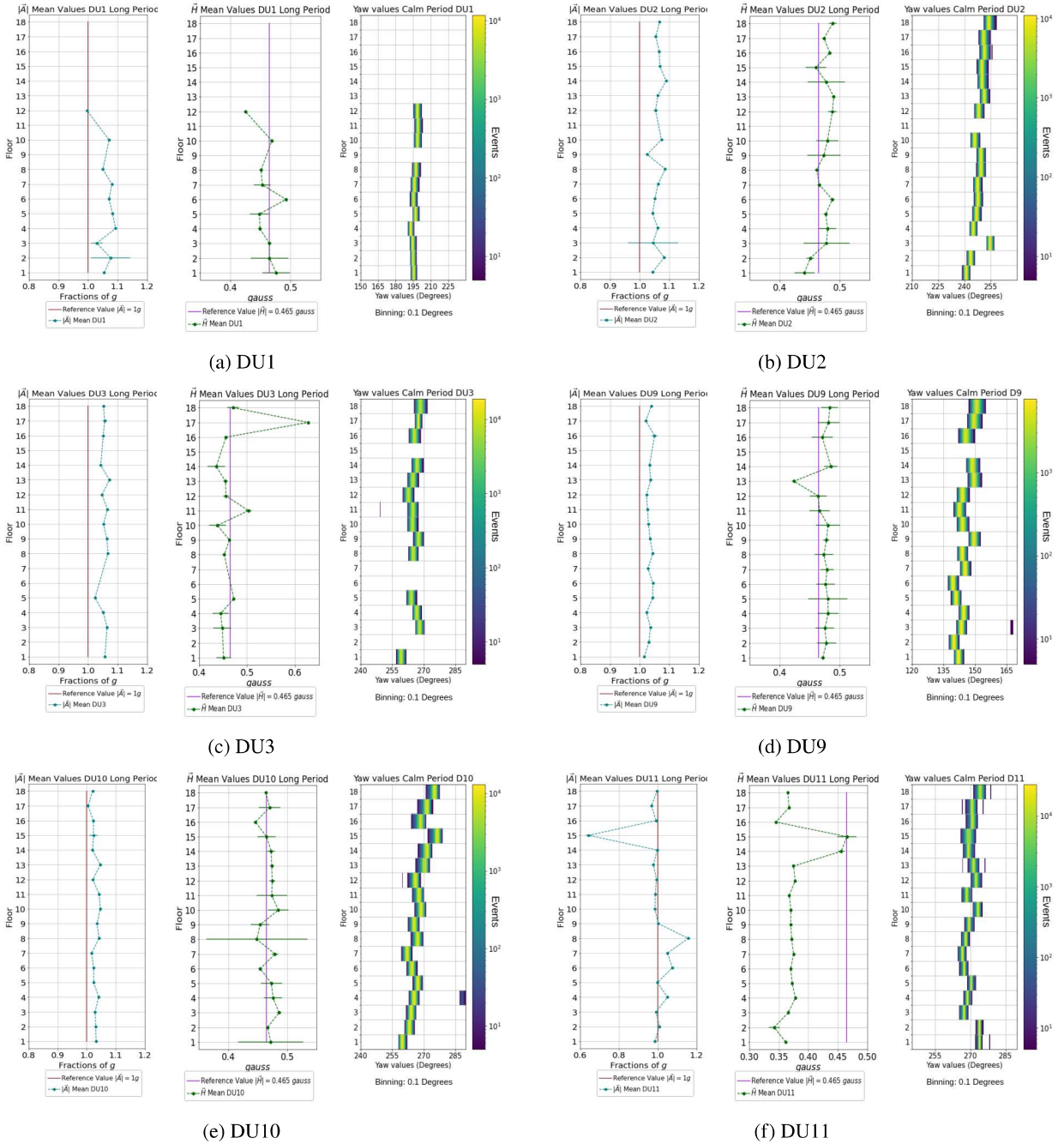


Figure 4.10: Mean values for $|\vec{A}|$, $|\vec{H}|$ and 2D orientation distributions for Yaw (Y) in compasses in ORCA6 for Short (Calm)-Period.

According to the form of YPR Equations, the ratios/products propagate \mathbf{A} and \mathbf{H} uncertainties. Then, the propagation of uncertainties for YPR is different from the propagation in $|\vec{\mathbf{A}}|$ and $|\vec{\mathbf{H}}|$. Given this, the magnitude of the shifts found in Y spread between nearby Floors has no relation with the $|\vec{\mathbf{A}}|$ or $|\vec{\mathbf{H}}|$ estimated values. The Y spread shifts are thus expected to be observed independently of the period observed, then, external contributions are not causing these shifts. The estimation of Y shifts lead to the global effect of (propagated) systematic uncertainties on Y data, it is represented in the next section, representing the main contribution of this work.

4.2.2 Preliminary parameterization of Systematic Uncertainties

Considering the mechanical model used in KM3NeT for line shape reconstruction⁴⁰, DOM positioning is influenced by horizontal and vertical drag forces (Figure 4.11a) generated by external factors (*i.e.* sea current), also, influencing the DOM orientation.

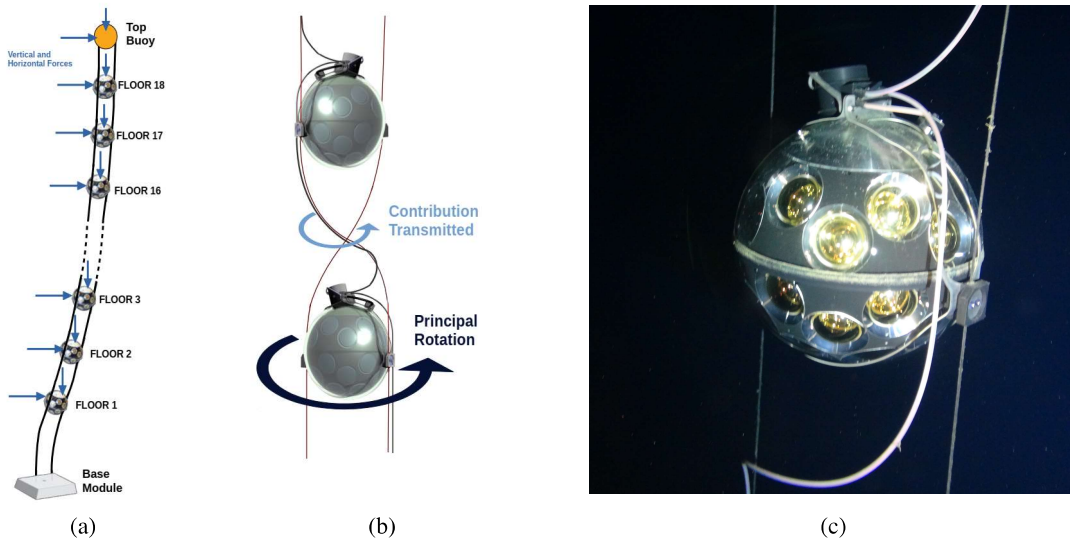


Figure 4.11: Considerations about DOM orientation. (a) Drag forces diagram acting on DU elements. (b) The individual rotations of a Floor is transmitted to nearby ones, due to cable stretching. (c) Each DOM is fixed in the DU structure by two metallic fibers.

The sea current has different directions along the year, the drag forces in the detectors vicinity vary, in general, horizontal forces magnitude is larger than vertical ones. Since each KM3NeT DU is implemented with a floating system that prevents the DU structure from collapsing, vertical drag forces are minimized and do not contribute to the DOM orientation changes. Besides, the DU structure keeps the 18 DOMs fixed using two metal fiber cables on the opposite sides of each DOM (Figure 4.11c). At the base of each DU, a fixed structure called "Base Module" maintain the metal fiber cables straight, in turn holding the 18 DOMs tight, at the top, there is a floating buoy. The horizontal drag forces are the principal sources of the external contributions to DOM positioning and orientation,

and their magnitude is more significant as the DU structure height increases, a statement, for instance, supporting what observed before on Y spread of F18, being broader than Y spread in F1.

Since sea current contributions to DOM orientation can differ, each Floor is subjected to individual horizontal forces. However, metallic fiber cables that hold the DOMs can propagate the rotations experienced from each DOM to nearby due to cables stretching (Figure 4.11b). The DOM rotation contribution to nearby Floors specifically refers to rotations concerning the z-axis only (Y contributions), according to the global reference system. Furthermore, these contributions are stronger when more significant the principal rotation (metallic fiber cables stretch more). Considering DOM orientation contributions by sea current are varied at different heights, then these "secondary" contributions may impact differently. Considering all secondary orientation contributions DOM can experience over time, it is possible that metal fiber cables stretching not only propagates rotation contributions but also tends to constrain the possible rotations. It is assumed in this work, the Y shifts are generated due to DOM orientation stability acquired by each DU, and the parameterization of such changes (residuals) is a main motivation. Hence, it is necessary to infer about a possible pattern for Y shifts independent of the sea current influence over DOM orientation in all DUs. The work is then focused to determine the magnitude of the changes affecting Y by defining a model that predicts Y shifts. Figure 4.12 represents the Y spread for all the ORCA6 DUs, it is expected that Y shifts pattern is conserved in both periods (Short and Long-Period). The cases of DU2F3, DU3F1, DU11F1-F2 does not represent a significant sample impacting statistics for a parameterization in a first attempt. In order to verify that Y shifts have the same trend independently of the period, a comparison based on the mean and mode of Y spreads of Short and Long-Period becomes appropriate. First, the statistical information needed for this comparison is shown in Tables A.2 - A.3. According to the results, the calculated mode (most representative Y) for ORCA6 compasses data is the same in both periods. The largest difference between Short and Long-Period modes is $\sim 0.3^\circ$. This result supports the assumption that the pattern associated with shifts is conserved over time, a similar comparison can be made using the mean instead of the mode from Y spreads, reaching the same conclusion. The mean is the estimator selected for the systematics analysis developed in this work.

The "stable orientation" is associated to the "nominal" orientation of the DOM, and can be characterized by the mean compass dataset for Y. A similar analysis for PR stresses the stability of each Floor along all DUs. As seen in Figure 4.12, it seems Y nominal increases systematically from F1 to F18 in all DUs, what may represents a manifestation that DU is twisted in the same direction (around z-axis). The Y nominal from the same DU is thus parameterized in this work, with a first order polynomial function (linear) as indicated. The Figures 4.13-4.14 represent the Linear parameterizations obtained when the mean and mode of Y for DU9 and DU11 are considered in Short and Long-Period (Tables A.2-A.3).

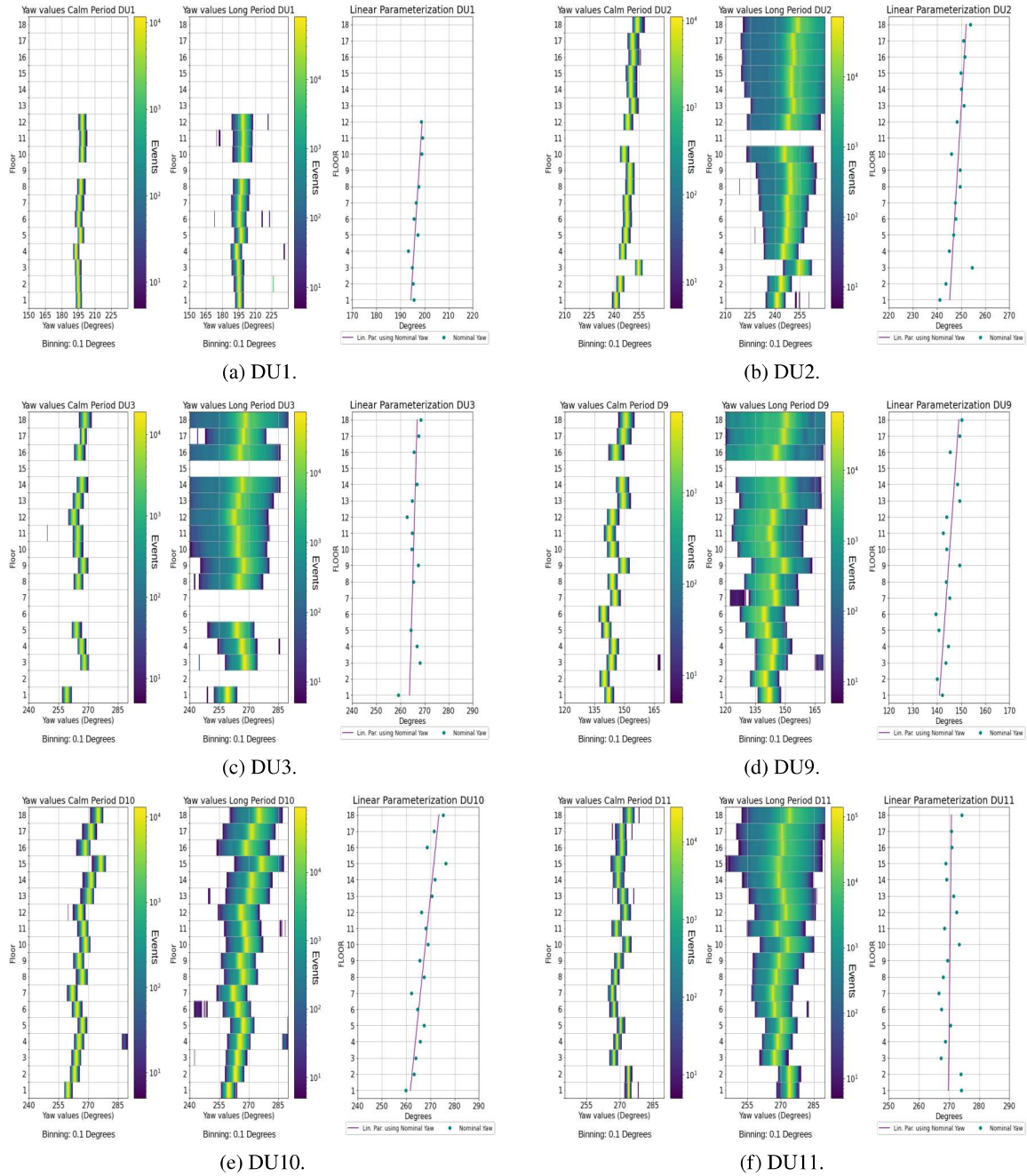


Figure 4.12: 2D orientation distribution for Yaw (Y), Short (Calm) and Long-Period, together Linear Parameterization of Y nominal values (Long-Period) in all ORCA6 DUs. Consolidated data selection is used.

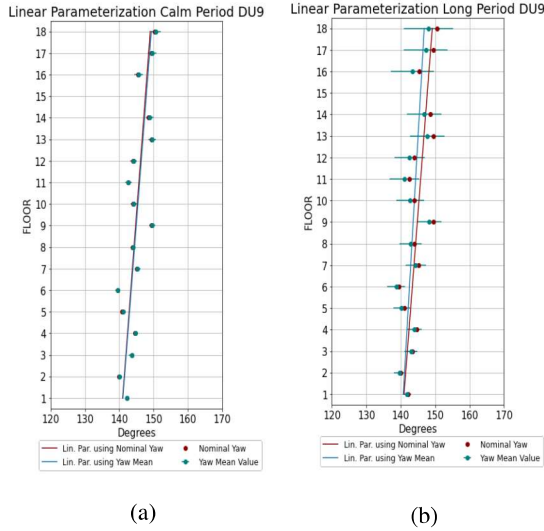


Figure 4.13: Linear Parameterizations for Y mean-mode values in DU9. (a) Short(Calm)-Period. (b) Long-Period.

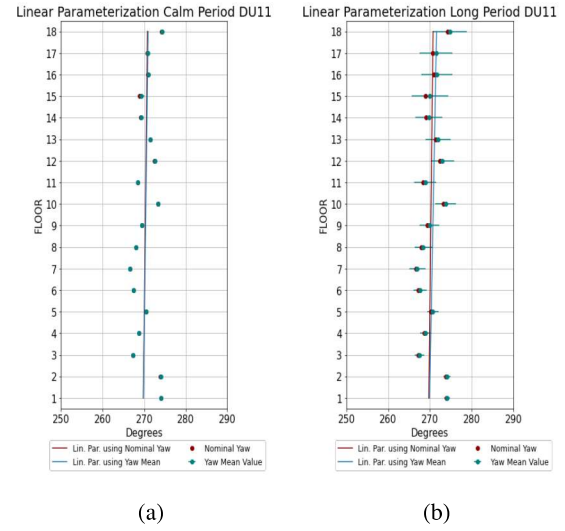


Figure 4.14: Linear Parameterizations for Y mean-mode values in DU11. (a) Short(Calm)-Period. (b) Long-Period.

As seen, linear parameterizations in both periods are equivalent, regardless mean or mode is used as estimator for Y, however, as commented, the mean is selected for our analysis. It is then convenient to express now the associated systematics (Y shifts) in terms of residuals, as Equation 4.1 refers.

$$\mathbf{Y}_{\text{res}} (\text{systematics}) = \mathbf{Y}_{\text{parameterized}} - \mathbf{Y}_{\text{data}} \quad (4.1)$$

The results of the implementation of \mathbf{Y}_{res} over \mathbf{Y}_{data} (mean) per DU-Floor are summarized in Tables A.4 - A.9 (Short-Period), \mathbf{Y}_{data} (mode) is only list for comparison. In particular, Table 4.1 shows Y final estimations ($\hat{\mathbf{Y}}$) from Equation 4.2, where $\bar{\mathbf{Y}}_{\text{data}}$ is the average of \mathbf{Y}_{data} , $\mathbf{SD}_{\mathbf{Y}\text{-data}}^{\text{stat}}$ is the Standard Deviation on \mathbf{Y}_{data} , and $\bar{\mathbf{Y}}_{\text{res}}^{\text{sys}}$ is the average of the absolute residuals \mathbf{Y}_{res} per DU. Propagation of uncertainties on \mathbf{Y}_{data} and $\mathbf{Y}_{\text{parameterized}}$ were assumed "negligible" (because the small size of the uncertainties observed) in this analysis.

$$\hat{\mathbf{Y}} = \bar{\mathbf{Y}}_{\text{data}} \pm \mathbf{SD}_{\mathbf{Y}\text{-data}}^{\text{stat}} \pm \bar{\mathbf{Y}}_{\text{res}}^{\text{sys}} \quad (4.2)$$

DU	\bar{Y}_{data}	$\text{SD}_{Y\text{-data}}^{\text{stat}}$	$\bar{Y}_{\text{res}}^{\text{sys}}$	$\text{SE}_{Y\text{-res}}^{\text{sys}}$
1	196.88	1.90	0.79	0.31
2	248.83	3.45	1.70	0.64
3	265.54	2.34	1.64	0.57
9	145.07	3.45	2.08	0.57
10	267.44	4.14	1.86	0.53
11	270.41	2.42	2.02	0.56

(a) Using Y mean values in Short-Period.

DU	\bar{Y}_{data}	$\text{SD}_{Y\text{-data}}^{\text{stat}}$	$\bar{Y}_{\text{res}}^{\text{sys}}$	$\text{SE}_{Y\text{-res}}^{\text{sys}}$
1	196.80	1.93	0.85	0.32
2	249.66	3.65	1.73	0.64
3	265.99	2.43	1.64	0.57
9	143.53	3.94	2.01	0.57
10	268.28	4.44	1.81	0.52
11	270.74	2.41	1.98	0.55

(b) Using Yaw mean values in Long-Period.

Table 4.1: $\bar{Y}_{\text{data}} - \bar{Y}_{\text{res}}$ averaged and $\text{SD}_{Y\text{-data}}^{\text{stat}}$ (Short and Long-Period) and their uncertainties for all ORCA6 DUs.

As appreciable in both periods (Short and Long), the results are statistically similar, the maximum difference found between results of both periods is $\sim 0.03^\circ$. Based on the associated systematics ($\bar{Y}_{\text{res}}^{\text{sys}}$), the compass accuracy is better than 2.08° , fulfilling the 3.5° for KM3NeT neutrino physics and astrophysics programs¹. The choice of the most suitable model to parameterize the DOM orientation along the same DU will depend on other comparative analyses that were not developed in this work.

4.2.3 Selection of compasses for online orientation monitoring

Based on the results of this work, in particular, regarding systematics, it is possible to identify the compasses with the best performance. Then, the best choices for online monitoring of the corresponding DU follows the next-considerations: compasses with smaller \bar{Y}_{res} , same Floors with similar \bar{Y}_{res} (compasses at some height) along the DU, and minimum 3 compasses per DU in order to monitor three specific sectors (bottom, middle, and top). Because the consolidated data selection in this work, the online compasses monitoring doesn't contemplate those higher than F12 in DU1. In this specific case, it is proposed to monitor a Floor that is not within the main selection. For ORCA6, the selection of F4, F8, and F17 is proposed for compass online monitoring. Figure 4.15 graphically shows the results obtained in the previous section. These results are also supported by the Gaussian distributions shown in Figure 4.16).

Yaw Values ORCA6 Long Period RUN 7221-8721

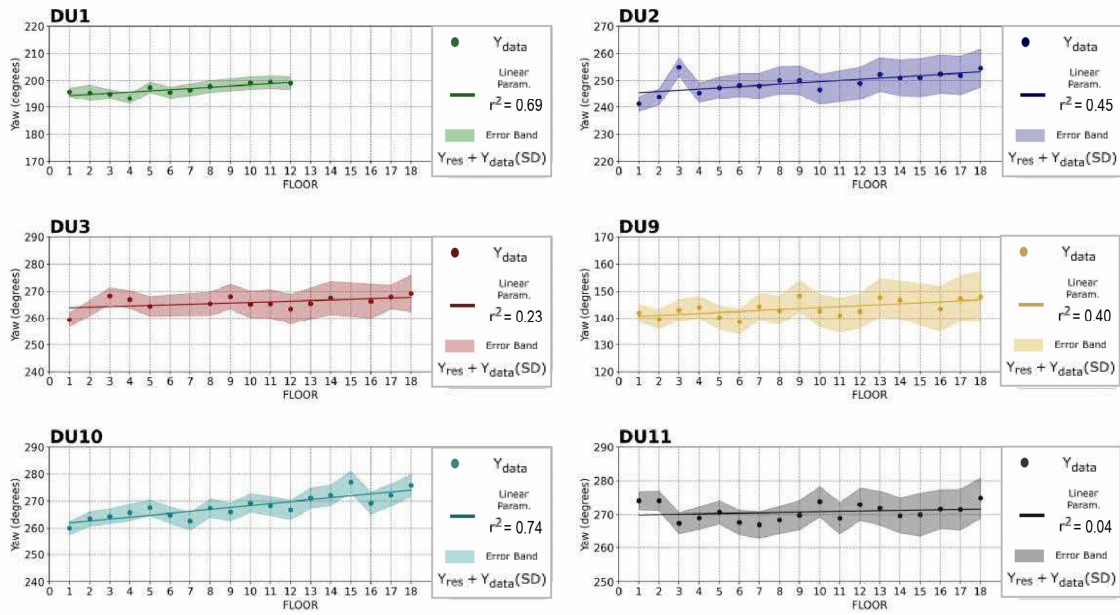


Figure 4.15: Error Band representation ($Y_{data}(\text{mean}) \pm Y_{res} \pm Y_{data}(SD)$) and Linear parameterized of Y_{data} in Long-Period estimated in this work.

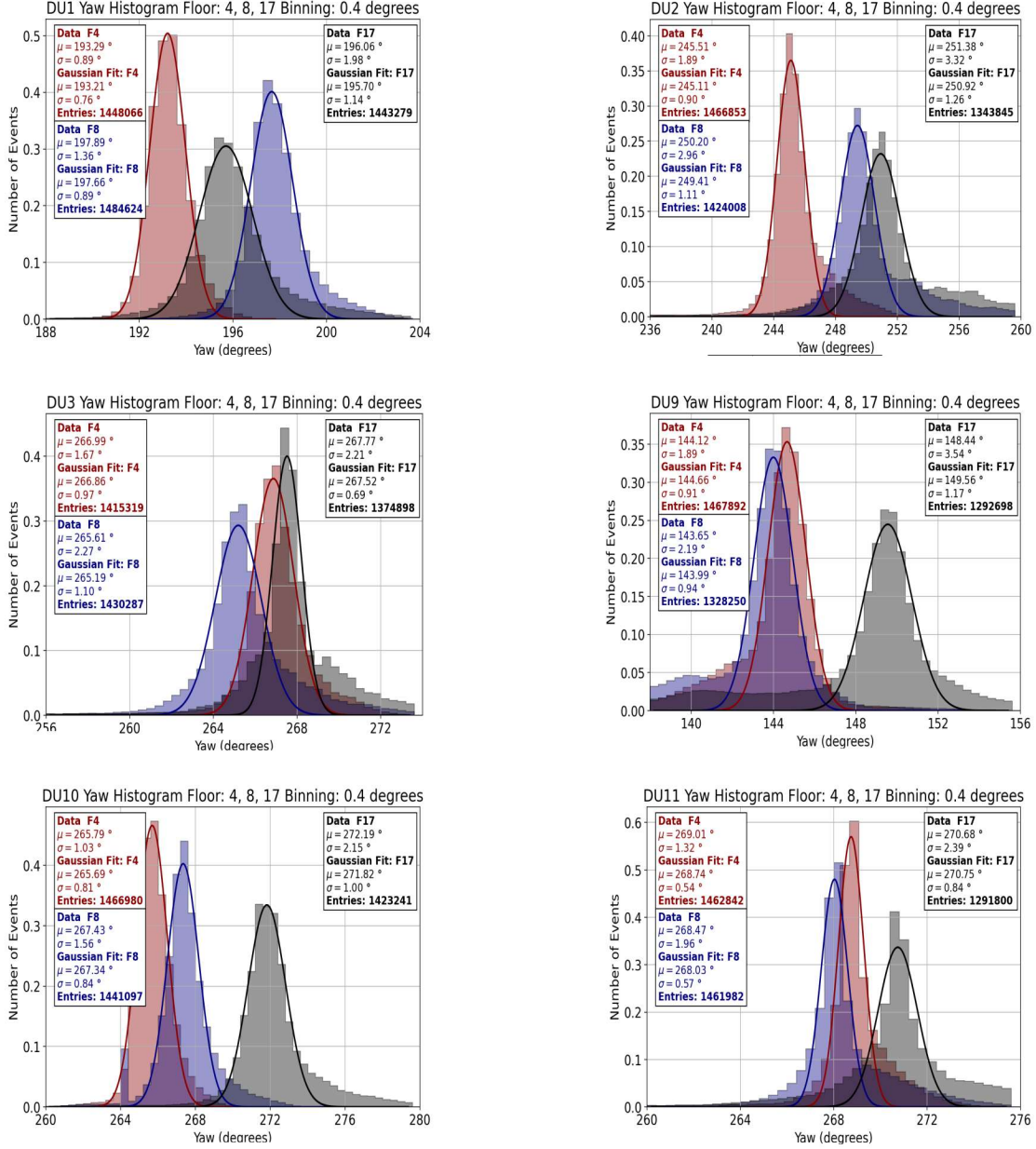


Figure 4.16: Gaussian distributions of reconstructed Y for DU1, DU2, DU3, DU9, DU10 and DU11 in Long-Period dataset of ORCA6.

4.3 Other Contributions to the compass calibration scheme

Along the development of this work, opportunities for improving the routines of compasses calibration arose. The following subsections explain further contributions beyond the main goal of this work (compasses systematics).

4.3.1 Data Quality from DB

Each DU element is labeled along testing routines (Lab, Dark Room, etc.). If the DU elements pass the corresponding tests, they are implemented in the corresponding detector site (*in-situ*). Referring specifically to the compass, at DB, there are compass data available from online and offline tests. Having control of the compass data sent to the DB, it allows to verify the compatibility between settings configured in the DM and the intrinsic operation of DUs compasses (at the lab and deployed at the detector site). To control the compass data stream features, a Python-based script was developed. Once the compass data is retrieved from the DB by selecting the appropriate period and source (off-site/on-site), the script is able to estimate the amount of unexpected data (zeros or NaN). The algorithm doesn't quantify the number of duplicates stored in the dataset but manipulation. Figure 4.17 shows the script output in the shell for a sample of compass data. Additionally, the script also generates 2D histograms of the compass data distribution over time.

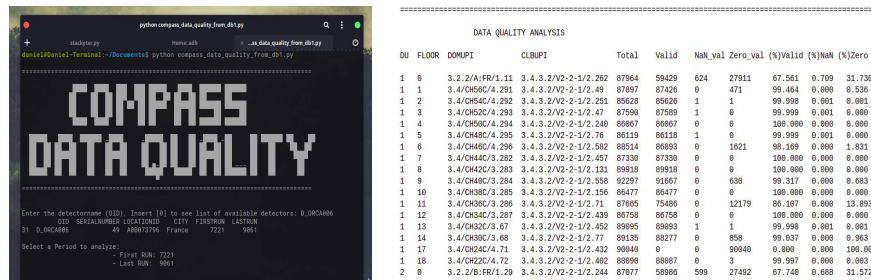


Figure 4.17: Interface and outputs of compass data quality script. The script shows by percentage the amount of 0, NaN and raw compass data available in the retrieved dataset.

The performance and reach of this script is subject of improvements and feedback by KM3NeT experts[‡].

4.3.2 Calibration file checks

Once the compasses calibration has been carried out, calibration parameters are saved in a dedicated XML file, later on this file is sent to the DB. A specific compass can be associated with several calibration files. During the development of this work, it was proposed to use the most recent XML file available to properly calibrate the compass dataset. However, not all compass calibration files have a suitable format (corrupted files can appear). A script

[‡]<https://git.km3net.de/working-groups/daq/-/issues/116>

was developed to verify the health of the compass calibration files and verify the contained calibration parameters. Figure 4.18 shows the script output in the shell for a given group of compasses.

```

python compass_calib_file_check.py
-----
COMPASS CALIBRATION FILE CHECK
-----
Enter the detectorname (ID), insert (R) in our list of available detectors:
ID: 001 002 003 004 005 006 007 008 009 010 011 012 013 014 015 016 017 018 019 020
SI: 2_001A080 49 48807370 France 7221 9855
Organizing tables: 100 0% 001718

Error labels:
0 No column order vector
1 No row order vector
2 No vector order
3 Axis values not found
4 Axis values not found
5 Axis values not found
6 HOFF values not found

IDID FIDIDSI COMPASS Test_Type_ver Content_sval Errors
0 1 0 3.4.3.4/AMBI/1292 v3 No Data
1 1 1 3.4.3.4/AMBI/1311 v3 v2
2 1 2 3.4.3.4/AMBI/1311 v3 v2
3 1 3 3.4.3.4/AMBI/1311 v3 v2
4 1 4 3.4.3.4/AMBI/1240 v3 v2
5 1 5 3.4.3.4/AMBI/1240 v3 v2
6 1 6 3.4.3.4/AMBI/1382 v3 v2
7 1 7 3.4.3.4/AMBI/1422 v3 v2
8 1 8 3.4.3.4/AMBI/1311 v3 v2
9 1 9 3.4.3.4/AMBI/1384 v3 No Data
10 1 10 3.4.3.4/AMBI/1384 v3 v2
11 1 11 3.4.3.4/AMBI/1311 v3 v2
12 1 12 3.4.3.4/AMBI/1311 v3 v2
13 1 13 3.4.3.4/AMBI/1422 v3 v2
14 1 14 3.4.3.4/AMBI/1311 v3 v2
15 1 15 3.4.3.4/AMBI/1311 v3 v2
16 1 16 3.4.3.4/AMBI/1311 v3 v2
17 1 17 3.4.3.4/AMBI/1422 v3 v2
18 1 18 3.4.3.4/AMBI/1422 v3 v2
19 2 0 3.4.3.4/AMBI/1244 v3 No Data

```

Figure 4.18: Interface and outputs of compass calibration file check script. The script easily verifies the sanity of compass calibration files.

4.3.3 Compass testing in the Dark Room

The compasses tests in the "Dark Room" are based on setting the compass board in 4 referential orientations: 0° , 90° , 180° , and 270° to Magnetic North (keeping the compass board horizontally). Once the compass data (accelerometer/magnetometer) is obtained in these four reference orientations, the Y values are calculated with the corresponding calibrated parameters. The residuals obtained from the difference between the referential orientations and the values from calibrated compass data are considered. If some residual becomes greater than 3.5° (minimum accuracy expected for calibrated compasses), the calibration procedure is considered unsuccessful⁶. At the beginning of this work, the routine of this verification needed some improvements. The routine was then entirely rewritten in C++ to improve the software's compatibility and avoid software environment conflicts reported by the operators using the former routine. Figure 4.19 shows the script output run in the shell over data of a given compass.

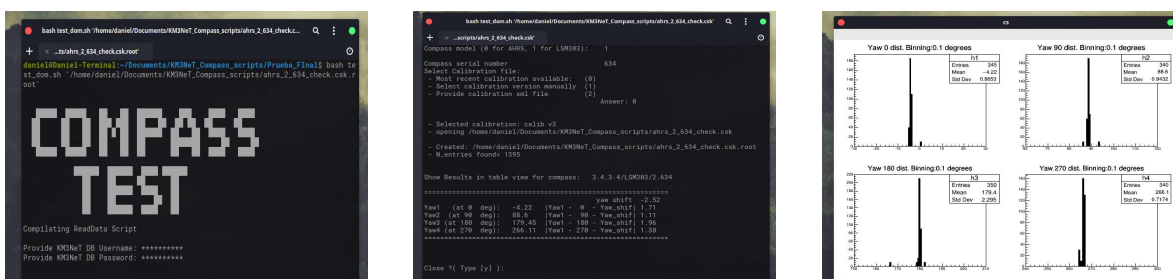


Figure 4.19: Interface and outputs of compass testing script Dark Room setups.

The implementations developed in the compass test software for Dark Room DU setups were already considered for future implementation in the official KM3NeT software[§].

[§]<https://git.km3net.de/bdarquea/compass-data-analysis/-/issues/1>

Chapter 5

Conclusions and Future Work

5.1 Conclusions:

KM3NeT is a long-term multidisciplinary infrastructure incorporating two neutrino telescopes: ARCA and ORCA. The compass positioning subsystem is in charge of determining the orientation of the DOM (arranged along the DUs). Each compass board consists of 3D-accelerometer and 3D-magnetometer to determine the orientation. The DOM orientation accuracy required for the successful reconstruction of directionality of neutrino-like events is $< 3.5^\circ$. Main conclusions of this work are as follow:

- The analysis developed about compass performances indicates that the systematics ($< 3.5^\circ$) required for the success of the KM3NeT physics goals is satisfied for the current state of the ORCA detector. Results of this work delivered an $\sim 2.08^\circ$ of associated systematics.

This was possible thanks to the following technical achievements:

- New filtering conditions for compass data proposed to improve their, with a remarkable improvement regarding default filtering.
- Compass data communication sanity checks were carried out. In this sense, a set of scripts were developed: data quality analysis, compass calibration file check, compass test in the dark room and compass data analysis.

From the physics and statistical data analysis perspective:

- The $|\vec{\mathbf{A}}|$ and $|\vec{\mathbf{H}}|$ vector modulus estimates the uncertainties related to each compass accelerometer and magnetometer. However, this may not be related to the global effect propagated in the equations used for reconstruction of orientation (YPR).
- It is verified that $|\vec{\mathbf{A}}|$ and $|\vec{\mathbf{H}}|$ does not vary representatively in time regardless of orientation. $|\vec{\mathbf{H}}|$ may be slightly affected due to local magnetic interference, or an undetermined scale factor is needed.

- Y values can be estimated independently of the period and external effects on orientation, averaged with data of a selected period, and define nominal orientation.
- Nominal Y values can be parameterized with a predefined model in such a way that the residuals found give an idea of the associated systematics, not compensated by calibration of the compasses.
- For ORCA6 detector the F4, F8 and F17 show the lesser systematic influence according to the developed Linear Parameterization.

From the consolidated data selection analysis, the Short-Period (stable orientation, weak interaction with external influences, *e.g.*, sea current) and Long-Period (highly influenced by sea current) deliver compatible results regarding systematics (the same is expected in random periods). In this sense, the experimental methodology in this work is independent of the selected period, and independent of external influences.

5.2 Future Work:

During the work, different aspects were found that must be considered to improve both the current calibration procedures of compasses, the understanding of the communication scheme, and the storage of compass data. This work considered only compass data from the ORCA6 detector (6DUs), however, is reproducible for other ORCA and ARCA detector layouts. From the DU mechanical model point of view (did not discussed in this work), the systematics identification is possible due to the nominal orientation acquired by the mechanical stability of the DU elements at the detector site. For future works, it is proposed to develop a similar analysis beyond the linear parameterization model to estimate systematics and a better/robust estimator as the χ^2 (instead r^2). Additionally, similar parameterization models can be included in P and R nominal values. Considering that Y values include the uncertainties of P and R, it is expected that the systematic uncertainties of P and R to be lower than the estimated uncertainties for Y. A more rigorous considerations on Y residuals components uncertainties propagation are also proposed. Furthermore upgraded tools are being developed for future compasses that will be deployed in ORCA and ARCA detectors (hardware and software). The task of verifying that the corresponding calibration files are saved in the appropriate format is proposed to future researchers. The testing of the final Y estimation, with its uncertainties, in the mechanical model and line shape reconstruction algorithm, is an important activity could be done in an advanced phase of this study.

Appendix A

Figures and Tables

The frequency for recorded events and compasses communication over over Long-Period (RUN 7721-8721) are shown in Figures A.1 and A.2.

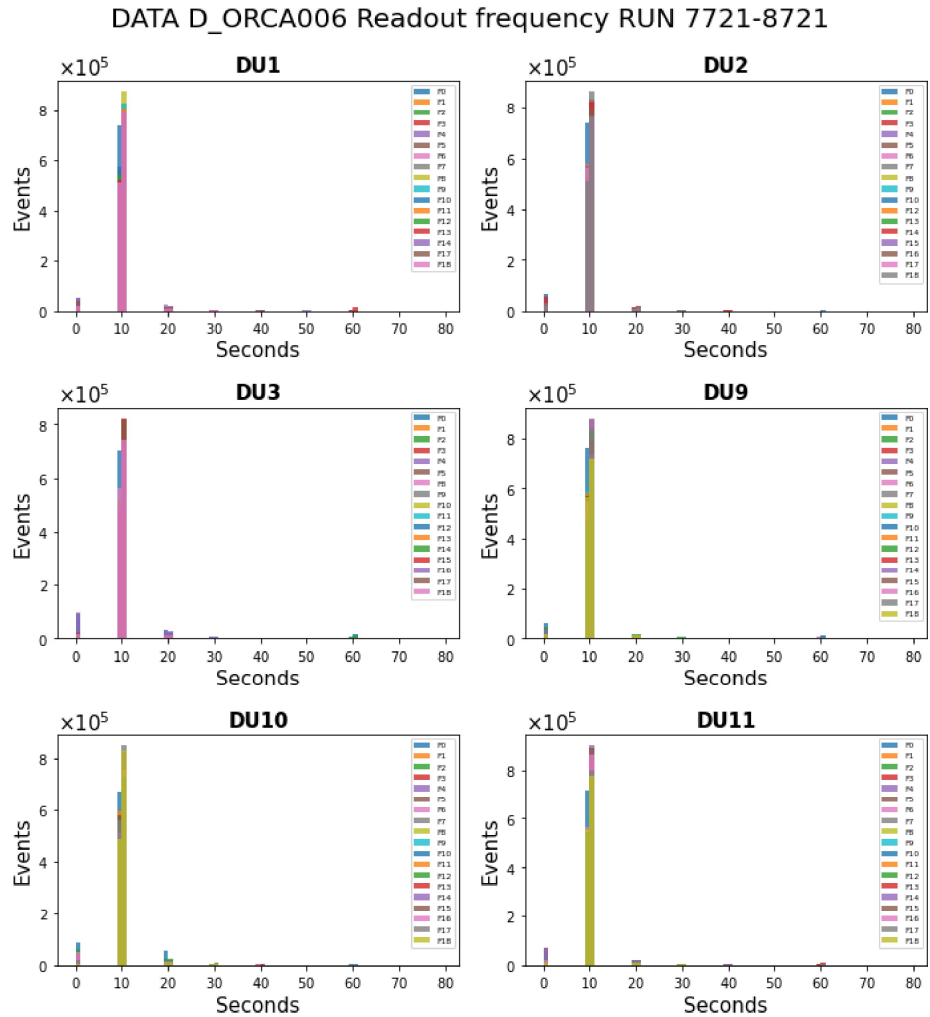


Figure A.1: Estimated compass recording frequency for Long-Period, considering all compasses in ORCA6. The recording frequency can be estimated by the time differences mode, calculated as the time difference of consecutive events in the dataset.

Figure A.1 shows the estimated recording frequency (time difference between consecutive measurements), around 10 seconds in all histograms, as expected.

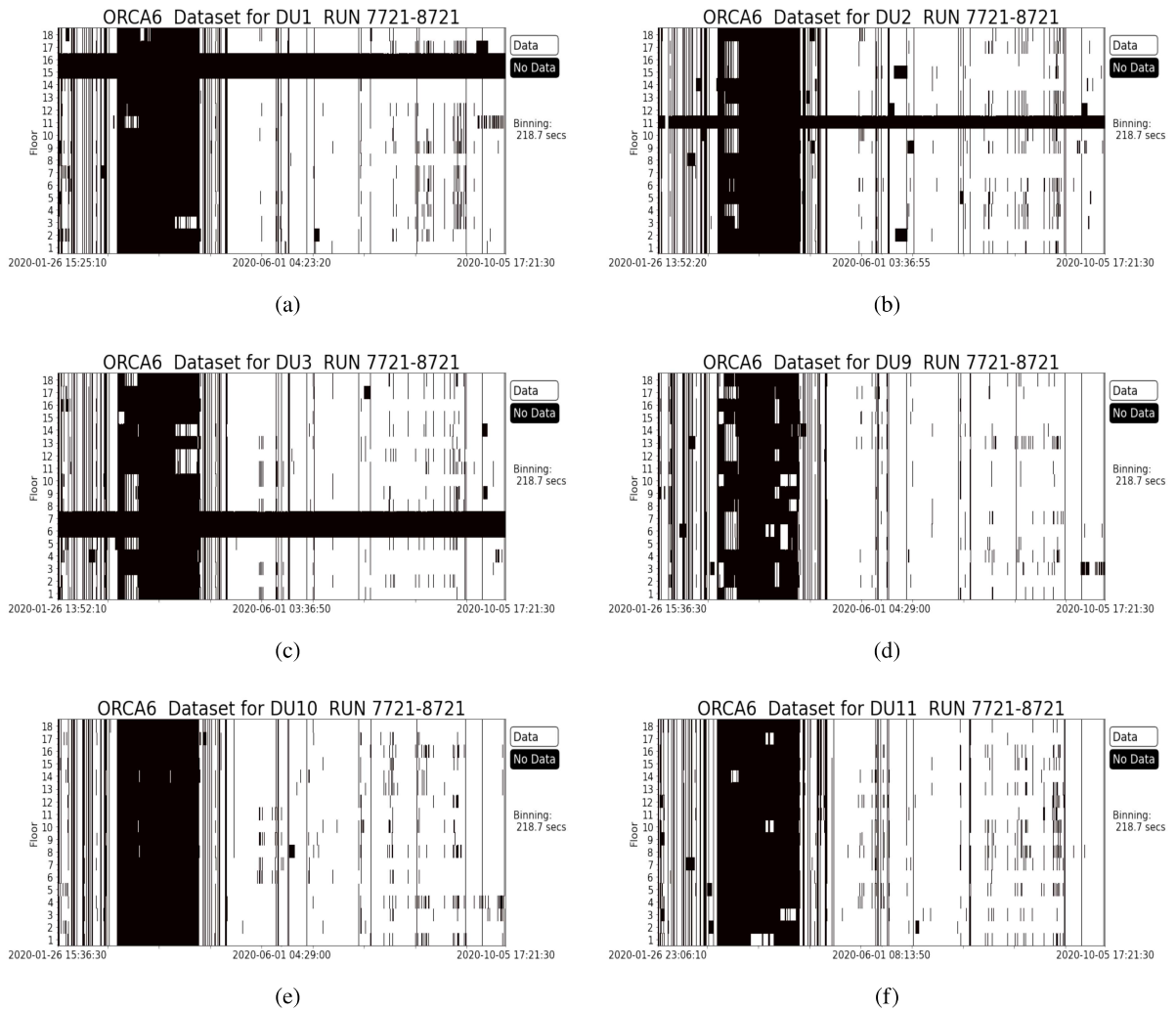


Figure A.2: Distribution of compass communication data over time for Long-Period, considering all compasses in ORCA6. It is obtained using the UNIXTIME parameter of each compass event recorded in DB.

As seen in Figure A.2, in some cases, data is almost absent in the entire period (*i.e.* F16 and 15 DU1 Figure A.2a), but it is because Floors were turned off during this period and data was not recorded until to develop a technical solution to be implemented. The absence of compass data can also happen due to DOM unexpected operational errors. In general, all compasses can show no uniform communications. During this work, this incident was reported through the KM3NeT git* for subsequent crosscheck diagnosis.

*<https://git.km3net.de/working-groups/daq/issues/105>

Table A.1: Mean, Standard Deviation (SD) and Percentage change (%) with respect to the reference values of $|\vec{A}|$ and $|\vec{H}|$ (fractions of g and *gauss* respectively) for ORCA6 compasses in Long-Period.

DU	FLOOR	Mean $ \vec{A} $	Mean $ \vec{H} $	SD $ \vec{A} $	SD $ \vec{H} $	% Variation with Ref. $ \vec{A} $	% Variation with Ref. $ \vec{H} $	DU	FLOOR	Mean $ \vec{A} $	Mean $ \vec{H} $	SD $ \vec{A} $	SD $ \vec{H} $	% Variation with Ref. $ \vec{A} $	% Variation with Ref. $ \vec{H} $
1	1	1.05	0.48	0.00	0.02	5.47	2.40	9	7	1.03	0.48	0.00	0.01	2.78	2.97
1	2	1.08	0.47	0.07	0.03	7.69	0.03	9	8	1.04	0.47	0.00	0.02	4.44	1.88
1	3	1.03	0.47	0.02	0.00	2.94	0.01	9	9	1.04	0.48	0.00	0.01	3.51	2.79
1	4	1.09	0.45	0.00	0.00	9.33	3.38	9	10	1.03	0.48	0.00	0.02	2.96	3.35
1	5	1.08	0.45	0.00	0.02	8.27	3.59	9	11	1.03	0.47	0.00	0.02	2.64	0.34
1	6	1.07	0.49	0.00	0.00	7.11	5.94	9	12	1.02	0.46	0.00	0.01	2.33	0.16
1	7	1.08	0.45	0.00	0.01	8.06	2.58	9	13	1.04	0.42	0.00	0.00	3.72	8.89
1	8	1.05	0.45	0.00	0.00	5.04	2.96	9	14	1.03	0.49	0.00	0.01	3.33	4.41
1	10	1.07	0.47	0.00	0.00	7.10	0.85	9	16	1.05	0.47	0.01	0.02	5.03	1.28
1	12	1.00	0.43	0.00	0.00	0.38	8.57	9	17	1.02	0.48	0.00	0.02	2.10	3.57
2	1	1.04	0.44	0.00	0.02	4.40	5.10	9	18	1.04	0.48	0.00	0.01	3.90	3.90
2	2	1.08	0.45	0.00	0.01	8.29	2.99	10	1	1.03	0.47	0.00	0.06	3.24	1.55
2	3	1.05	0.48	0.08	0.04	4.51	2.81	10	2	1.03	0.47	0.00	0.00	3.10	0.41
2	4	1.06	0.48	0.00	0.01	6.13	3.22	10	3	1.03	0.49	0.00	0.00	2.85	4.59
2	5	1.04	0.48	0.00	0.00	4.35	2.53	10	4	1.04	0.48	0.00	0.02	4.13	2.38
2	6	1.05	0.49	0.00	0.00	5.18	4.88	10	5	1.02	0.47	0.00	0.02	2.40	1.76
2	7	1.06	0.47	0.00	0.00	6.22	0.25	10	6	1.02	0.45	0.00	0.00	2.33	2.29
2	8	1.09	0.46	0.00	0.00	8.63	0.69	10	7	1.02	0.48	0.00	0.01	1.69	3.12
2	9	1.03	0.47	0.00	0.03	2.56	1.86	10	8	1.04	0.45	0.00	0.09	4.21	3.55
2	10	1.07	0.48	0.00	0.02	7.35	3.15	10	9	1.04	0.45	0.00	0.02	3.55	2.32
2	12	1.05	0.49	0.01	0.01	5.37	4.94	10	10	1.05	0.49	0.00	0.02	4.68	4.33
2	13	1.06	0.49	0.00	0.00	6.18	5.41	10	11	1.04	0.47	0.00	0.03	4.28	1.90
2	14	1.09	0.48	0.00	0.03	8.92	2.73	10	12	1.02	0.47	0.00	0.01	2.10	2.07
2	15	1.07	0.46	0.00	0.02	6.80	0.99	10	13	1.05	0.47	0.00	0.00	4.69	1.92
2	16	1.07	0.48	0.00	0.00	6.60	4.00	10	14	1.02	0.47	0.00	0.01	1.98	1.71
2	17	1.05	0.47	0.00	0.00	5.45	1.92	10	15	1.02	0.47	0.02	0.02	2.33	0.01
2	18	1.07	0.49	0.00	0.01	6.71	5.07	10	16	1.02	0.45	0.00	0.00	2.30	4.01
3	1	1.06	0.45	0.00	0.02	5.72	3.02	10	17	1.00	0.47	0.00	0.02	0.42	1.13
3	3	1.06	0.45	0.00	0.02	6.42	3.63	10	18	1.02	0.46	0.00	0.00	2.04	0.24
3	4	1.05	0.44	0.00	0.02	5.16	4.34	11	1	0.99	0.36	0.00	0.00	1.41	22.26
3	5	1.02	0.47	0.00	0.00	2.34	1.56	11	2	1.01	0.34	0.00	0.01	0.91	26.40
3	8	1.07	0.45	0.00	0.00	6.70	2.70	11	3	0.99	0.37	0.01	0.00	0.89	21.29
3	9	1.06	0.46	0.00	0.00	6.37	0.38	11	4	1.05	0.38	0.00	0.00	5.00	18.68
3	10	1.05	0.44	0.00	0.02	5.21	5.82	11	5	1.00	0.37	0.00	0.00	0.19	19.82
3	11	1.07	0.50	0.00	0.01	6.53	8.18	11	6	1.08	0.37	0.01	0.00	7.51	20.41
3	12	1.05	0.46	0.00	0.01	4.74	1.93	11	7	1.05	0.38	0.00	0.00	5.02	19.33
3	13	1.07	0.45	0.00	0.00	7.24	2.17	11	8	1.16	0.37	0.01	0.00	15.70	20.06
3	14	1.04	0.44	0.00	0.02	4.28	6.30	11	9	1.00	0.37	0.00	0.00	0.27	20.33
3	16	1.05	0.46	0.00	0.00	5.13	1.98	11	10	0.99	0.37	0.01	0.00	1.41	20.28
3	17	1.06	0.63	0.01	0.00	5.63	35.05	11	11	0.99	0.37	0.00	0.00	1.34	20.95
3	18	1.05	0.47	0.00	0.01	5.24	1.18	11	12	0.99	0.38	0.00	0.00	0.62	18.73
9	1	1.02	0.47	0.00	0.00	1.60	1.51	11	13	0.98	0.38	0.00	0.00	2.23	19.35
9	2	1.03	0.48	0.00	0.02	3.13	2.78	11	14	1.00	0.46	0.00	0.01	0.24	1.96
9	3	1.04	0.48	0.00	0.02	3.64	2.24	11	15	0.64	0.47	0.02	0.02	35.62	0.08
9	4	1.02	0.48	0.00	0.02	2.33	3.43	11	16	0.99	0.35	0.00	0.00	0.84	25.76
9	5	1.04	0.48	0.00	0.03	4.40	3.28	11	17	0.97	0.37	0.00	0.00	3.24	20.95
9	6	1.04	0.48	0.00	0.02	4.47	2.50	11	18	1.00	0.37	0.00	0.00	0.32	21.48

Table A.2: $Y_{\text{data}}(\text{mean})$, $Y_{\text{data}}(\text{SD})$ and $Y_{\text{data}}(\text{mode})$ in estimated from compass data in **Short-Period**. All quantities are represented in degrees.

DU	FLOOR	$Y_{\text{data}}(\text{mean})$	$Y_{\text{data}}(\text{SD})$	$Y_{\text{data}}(\text{mode})$	DU	FLOOR	$Y_{\text{data}}(\text{mean})$	$Y_{\text{data}}(\text{SD})$	$Y_{\text{data}}(\text{mode})$
1	1	195.78	0.66	195.6	9	7	145.36	0.77	145.2
1	2	195.30	0.66	195.2	9	8	144.05	0.79	143.8
1	3	194.97	0.66	194.8	9	9	149.61	0.90	149.4
1	4	193.26	0.75	193.2	9	10	144.22	0.94	144.0
1	5	197.42	0.69	197.2	9	11	142.67	0.96	142.6
1	6	195.58	0.74	195.6	9	12	144.15	0.96	144.0
1	7	196.44	0.80	196.5	9	13	149.59	1.01	149.4
1	8	197.77	0.74	197.5	9	14	148.84	1.08	148.5
1	10	199.02	0.73	198.8	9	16	145.68	1.24	145.4
1	11	199.45	0.75	199.1	9	17	149.63	1.21	149.4
1	12	199.02	0.79	198.7	9	18	150.76	1.42	150.3
2	1	241.13	0.60	241.1	10	1	259.93	0.52	259.9
2	2	243.68	0.59	243.6	10	2	263.30	0.55	263.2
2	3	254.73	0.58	254.6	10	3	264.16	0.57	264.0
2	4	245.11	0.57	245.1	10	4	265.60	1.54	265.7
2	5	247.02	0.67	246.9	10	5	267.29	0.55	267.4
2	6	247.82	0.61	247.8	10	6	264.50	0.65	264.6
2	7	247.54	0.61	247.5	10	7	262.20	0.60	262.1
2	8	249.51	0.67	249.5	10	8	267.15	0.64	267.4
2	9	249.50	0.63	249.5	10	9	265.56	0.62	265.5
2	10	245.96	0.66	245.9	10	10	268.80	0.61	268.9
2	12	248.23	0.66	248.2	10	11	267.80	0.64	268.0
2	13	251.40	0.66	251.2	10	12	266.11	0.65	266.3
2	14	250.16	0.67	250.0	10	13	270.48	0.70	270.5
2	15	250.08	0.72	249.9	10	14	271.56	0.67	271.8
2	16	251.55	0.74	251.4	10	15	276.46	0.67	276.3
2	17	251.07	0.73	251.0	10	16	268.60	0.71	268.7
2	18	254.00	0.72	253.9	10	17	271.57	0.71	271.5
3	1	259.33	0.56	259.2	10	18	275.19	0.65	275.3
3	3	268.15	0.56	268.1	11	1	274.05	0.23	274.0
3	4	266.79	0.57	266.8	11	2	274.00	0.26	273.9
3	5	264.19	0.60	264.4	11	3	267.33	0.32	267.3
3	8	265.14	0.62	265.4	11	4	268.79	0.28	268.7
3	9	267.63	0.60	267.4	11	5	270.44	0.30	270.4
3	10	264.77	0.60	264.6	11	6	267.40	0.30	267.4
3	11	264.96	0.64	264.9	11	7	266.66	0.32	266.6
3	12	262.83	0.67	262.7	11	8	268.08	0.33	268.0
3	13	264.95	0.65	264.8	11	9	269.47	0.36	269.4
3	14	266.94	0.63	266.8	11	10	273.37	0.38	273.3
3	16	265.69	0.67	265.5	11	11	268.49	0.39	268.4
3	17	267.53	0.43	267.5	11	12	272.57	0.42	272.5
3	18	268.50	0.70	268.5	11	13	271.50	0.43	271.4
9	1	142.27	0.63	142.2	11	14	269.25	0.44	269.2
9	2	140.08	0.67	140.0	11	15	269.30	0.78	268.9
9	3	143.65	0.83	143.6	11	16	271.04	0.47	270.9
9	4	144.73	0.69	144.6	11	17	270.88	0.46	270.8
9	5	141.09	0.70	140.8	11	18	274.32	0.53	274.2
9	6	139.60	0.74	139.5					

Table A.3: $Y_{\text{data}}(\text{mean})$, $Y_{\text{data}}(\text{SD})$ and $Y_{\text{data}}(\text{mode})$ in estimated from compass data in **Long-Period**. All quantities are represented in degrees.

DU	FLOOR	$Y_{\text{data}}(\text{mean})$	$Y_{\text{data}}(\text{SD})$	$Y_{\text{data}}(\text{mode})$	DU	FLOOR	$Y_{\text{data}}(\text{mean})$	$Y_{\text{data}}(\text{SD})$	$Y_{\text{data}}(\text{mode})$
1	1	195.79	0.75	195.6	9	7	144.34	2.94	145.3
1	2	195.43	2.11	195.1	9	8	142.89	3.19	143.9
1	3	195.01	0.89	194.7	9	9	148.27	3.63	149.5
1	4	193.29	0.97	193.2	9	10	142.75	4.00	144.0
1	5	197.50	1.06	197.2	9	11	141.06	4.29	142.5
1	6	195.65	1.20	195.6	9	12	142.57	4.40	144.0
1	7	196.51	1.37	196.4	9	13	147.76	5.02	149.5
1	8	197.89	1.36	197.4	9	14	146.78	4.98	148.7
1	10	199.16	1.48	198.8	9	16	143.42	6.32	145.4
1	11	199.54	1.50	199.1	9	17	147.34	6.36	149.5
1	12	199.13	1.60	198.7	9	18	148.04	7.15	150.6
2	1	241.29	1.10	241.0	10	1	260.04	0.68	259.9
2	2	243.94	1.37	243.6	10	2	263.48	0.83	263.3
2	3	255.04	1.62	254.6	10	3	264.39	0.93	264.1
2	4	245.47	1.97	245.1	10	4	265.81	1.27	265.7
2	5	247.45	2.31	246.8	10	5	267.60	1.06	267.4
2	6	248.31	2.59	247.6	10	6	264.86	1.29	264.7
2	7	248.11	2.91	247.4	10	7	262.60	1.34	262.1
2	8	250.17	3.40	249.3	10	8	267.42	1.58	267.4
2	9	250.14	3.61	249.3	10	9	266.03	1.53	265.5
2	10	246.70	3.92	245.7	10	10	269.31	1.59	268.9
2	12	249.00	4.32	248.1	10	11	268.29	1.61	268.0
2	13	252.25	4.49	251.2	10	12	266.69	1.77	266.3
2	14	251.05	4.92	250.0	10	13	271.09	1.93	270.5
2	15	251.08	5.37	249.8	10	14	272.18	1.96	271.8
2	16	252.47	5.40	251.4	10	15	277.13	2.12	276.4
2	17	251.93	5.41	251.0	10	16	269.30	2.28	268.7
2	18	254.66	5.30	253.7	10	17	272.23	2.26	271.5
3	1	259.42	1.00	259.2	10	18	275.82	2.23	275.3
3	3	268.31	1.43	268.0	11	1	274.15	0.71	274.0
3	4	266.99	1.68	266.8	11	2	274.10	0.89	273.9
3	5	264.46	1.97	264.4	11	3	267.49	1.13	267.2
3	8	265.49	2.74	265.4	11	4	269.01	1.32	268.7
3	9	268.01	2.94	267.4	11	5	270.74	1.43	270.3
3	10	265.20	3.33	264.6	11	6	267.67	1.63	267.3
3	11	265.36	3.68	264.9	11	7	267.00	1.90	266.6
3	12	263.39	3.94	262.7	11	8	268.45	2.05	268.0
3	13	265.50	4.10	264.8	11	9	269.89	2.32	269.4
3	14	267.53	4.46	266.8	11	10	273.81	2.49	273.3
3	16	266.34	4.70	265.5	11	11	268.94	2.66	268.4
3	17	267.88	2.75	267.5	11	12	273.04	2.76	272.4
3	18	269.23	5.17	268.3	11	13	271.98	3.03	271.4
9	1	141.89	1.21	142.1	11	14	269.75	3.17	269.1
9	2	139.58	1.54	140.1	11	15	269.99	4.35	268.9
9	3	143.02	1.90	143.5	11	16	271.65	3.76	270.9
9	4	144.04	2.02	144.6	11	17	271.49	3.99	270.7
9	5	140.28	2.39	141.0	11	18	274.89	4.01	274.2
9	6	138.69	2.62	139.5					

In each Tables A.4 - A.9 are shown the following values for a specific DU: $Y_{\text{data}}(\text{mean})$, Yaw mean values from a compass dataset; $Y_{\text{data}}(\text{SD})$, the standard deviation of the set of Yaw mean values for a compass dataset; $Y_{\text{parameterized}}$, the parameterized Y according Linear model; and Y_{res} , the residual estimated for each compass. For comparison, Y mean and mode values used to estimate the parameterization.

Table A.4: Y_{res} for **DU1** in Short-Period (RUN 8000-8085). All quantities are represented in degrees.

(a) Using Yaw mean values.

DU	FLOOR	$Y_{\text{data}}(\text{mean})$	$Y_{\text{data}}(\text{SD})$	$Y_{\text{parameterized}}$	Y_{res}
1	1	195.78	0.66	194.39	-1.38
1	2	195.30	0.66	194.84	-0.47
1	3	194.97	0.66	195.28	0.31
1	4	193.26	0.75	195.72	2.47
1	5	197.42	0.69	196.17	-1.26
1	6	195.58	0.74	196.61	1.03
1	7	196.44	0.80	197.05	0.61
1	8	197.77	0.74	197.49	-0.28
1	10	199.02	0.73	198.38	-0.64
1	11	199.45	0.75	198.82	-0.62
1	12	199.02	0.79	199.27	0.24

(b) Using Nominal mode Yaw values.

DU	FLOOR	$Y_{\text{data}}(\text{mode})$	$Y_{\text{parameterized}}$	Y_{res}
1	1	195.6	194.32	-1.28
1	2	195.2	194.75	-0.45
1	3	194.8	195.17	0.37
1	4	193.2	195.60	2.40
1	5	197.2	196.02	-1.18
1	6	195.6	196.45	0.85
1	7	196.5	196.87	0.37
1	8	197.5	197.30	-0.20
1	10	198.8	198.15	-0.65
1	11	199.1	198.57	-0.53
1	12	198.7	199.00	0.30

Table A.5: Y_{res} for **DU2** in Short-Period (RUN 8000-8085). All quantities are represented in degrees.

(a) Using Yaw mean values.						(b) Using Nominal mode Yaw values.				
DU	FLOOR	$Y_{\text{data}}(\text{mean})$	$Y_{\text{data}}(\text{SD})$	$Y_{\text{parameterized}}$	Y_{res}	DU	FLOOR	$Y_{\text{data}}(\text{mode})$	$Y_{\text{parameterized}}$	Y_{res}
2	1	241.13	0.60	245.30	4.17	2	1	241.1	245.26	4.16
2	2	243.68	0.59	245.71	2.03	2	2	243.6	245.66	2.06
2	3	254.73	0.58	246.12	-8.61	2	3	254.6	246.07	-8.53
2	4	245.11	0.57	246.52	1.42	2	4	245.1	246.47	1.37
2	5	247.02	0.67	246.93	-0.09	2	5	246.9	246.87	-0.03
2	6	247.82	0.61	247.34	-0.48	2	6	247.8	247.28	-0.52
2	7	247.54	0.61	247.75	0.21	2	7	247.5	247.68	0.18
2	8	249.51	0.67	248.16	-1.35	2	8	249.5	248.08	-1.42
2	9	249.50	0.63	248.57	-0.94	2	9	249.5	248.49	-1.01
2	10	245.96	0.66	248.97	3.01	2	10	245.9	248.89	2.99
2	12	248.23	0.66	249.79	1.56	2	12	248.2	249.70	1.50
2	13	251.40	0.66	250.20	-1.20	2	13	251.2	250.10	-1.10
2	14	250.16	0.67	250.61	0.45	2	14	250.0	250.50	0.50
2	15	250.08	0.72	251.02	0.94	2	15	249.9	250.91	1.01
2	16	251.55	0.74	251.42	-0.12	2	16	251.4	251.31	-0.09
2	17	251.07	0.73	251.83	0.77	2	17	251.0	251.71	0.71
2	18	254.00	0.72	252.24	-1.76	2	18	253.9	252.12	-1.78

Table A.6: Y_{res} for **DU3** in Short-Period (RUN 8000-8085). All quantities are represented in degrees.

(a) Using Yaw mean values.						(b) Using Nominal mode Yaw values.				
DU	FLOOR	$Y_{\text{data}}(\text{mean})$	$Y_{\text{data}}(\text{SD})$	$Y_{\text{parameterized}}$	Y_{res}	DU	FLOOR	$Y_{\text{data}}(\text{mode})$	$Y_{\text{parameterized}}$	Y_{res}
3	1	259.33	0.56	263.79	4.46	3	1	259.2	263.79	4.59
3	3	268.15	0.56	264.17	-3.98	3	3	268.1	264.16	-3.94
3	4	266.79	0.57	264.36	-2.42	3	4	266.8	264.35	-2.45
3	5	264.19	0.60	264.56	0.36	3	5	264.4	264.53	0.13
3	8	265.14	0.62	265.13	-0.01	3	8	265.4	265.09	-0.31
3	9	267.63	0.60	265.32	-2.31	3	9	267.4	265.27	-2.13
3	10	264.77	0.60	265.51	0.75	3	10	264.6	265.46	0.86
3	11	264.96	0.64	265.71	0.75	3	11	264.9	265.64	0.74
3	12	262.83	0.67	265.90	3.06	3	12	262.7	265.83	3.13
3	13	264.95	0.65	266.09	1.14	3	13	264.8	266.01	1.21
3	14	266.94	0.63	266.28	-0.65	3	14	266.8	266.20	-0.60
3	16	265.69	0.67	266.67	0.97	3	16	265.5	266.57	1.07
3	17	267.53	0.43	266.86	-0.67	3	17	267.5	266.75	-0.75
3	18	268.50	0.70	267.05	-1.45	3	18	268.5	266.94	-1.56

Table A.7: Y_{res} for **DU9** in Short-Period (RUN 8000-8085). All quantities are represented in degrees.

(a) Using Yaw mean values.						(b) Using Nominal Yaw values.				
DU	FLOOR	$Y_{data}(mean)$	$Y_{data}(SD)$	$Y_{parameterized}$	Y_{res}	DU	FLOOR	$Y_{data}(mode)$	$Y_{parameterized}$	Y_{res}
9	1	142.27	0.63	141.07	-1.20	9	1	142.2	140.99	-1.21
9	2	140.08	0.67	141.56	1.47	9	2	140.0	141.47	1.47
9	3	143.65	0.83	142.04	-1.60	9	3	143.6	141.94	-1.66
9	4	144.73	0.69	142.53	-2.20	9	4	144.6	142.41	-2.19
9	5	141.09	0.70	143.02	1.93	9	5	140.8	142.89	2.09
9	6	139.60	0.74	143.51	3.91	9	6	139.5	143.36	3.86
9	7	145.36	0.77	144.00	-1.37	9	7	145.2	143.83	-1.37
9	8	144.05	0.79	144.48	0.43	9	8	143.8	144.31	0.51
9	9	149.61	0.90	144.97	-4.64	9	9	149.4	144.78	-4.62
9	10	144.22	0.94	145.46	1.24	9	10	144.0	145.25	1.25
9	11	142.67	0.96	145.95	3.27	9	11	142.6	145.73	3.13
9	12	144.15	0.96	146.44	2.28	9	12	144.0	146.20	2.20
9	13	149.59	1.01	146.92	-2.67	9	13	149.4	146.68	-2.72
9	14	148.84	1.08	147.41	-1.43	9	14	148.5	147.15	-1.35
9	16	145.68	1.24	148.39	2.71	9	16	145.4	148.10	2.70
9	17	149.63	1.21	148.88	-0.75	9	17	149.4	148.57	-0.83
9	18	150.76	1.42	149.36	-1.39	9	18	150.3	149.04	-1.26

Table A.8: Y_{res} for **DU10** in Short-Period (RUN 8000-8085). All quantities are represented in degrees.

(a) Using Yaw mean values.						(b) Using Nominal Yaw values.				
DU	FLOOR	$Y_{data}(mean)$	$Y_{data}(SD)$	$Y_{parameterized}$	Y_{res}	DU	FLOOR	$Y_{data}(mode)$	$Y_{parameterized}$	Y_{res}
10	1	259.93	0.52	261.73	1.80	10	1	259.9	261.73	1.83
10	2	263.30	0.55	262.42	-0.88	10	2	263.2	262.42	-0.78
10	3	264.16	0.57	263.11	-1.06	10	3	264.0	263.11	-0.89
10	4	265.60	1.54	263.79	-1.81	10	4	265.7	263.81	-1.89
10	5	267.29	0.55	264.48	-2.81	10	5	267.4	264.50	-2.90
10	6	264.50	0.65	265.17	0.66	10	6	264.6	265.19	0.59
10	7	262.20	0.60	265.85	3.65	10	7	262.1	265.89	3.79
10	8	267.15	0.64	266.54	-0.61	10	8	267.4	266.58	-0.82
10	9	265.56	0.62	267.23	1.66	10	9	265.5	267.27	1.77
10	10	268.80	0.61	267.91	-0.89	10	10	268.9	267.96	-0.94
10	11	267.80	0.64	268.60	0.80	10	11	268.0	268.66	0.66
10	12	266.11	0.65	269.29	3.18	10	12	266.3	269.35	3.05
10	13	270.48	0.70	269.97	-0.51	10	13	270.5	270.04	-0.46
10	14	271.56	0.67	270.66	-0.90	10	14	271.8	270.73	-1.07
10	15	276.46	0.67	271.35	-5.11	10	15	276.3	271.43	-4.87
10	16	268.60	0.71	272.03	3.43	10	16	268.7	272.12	3.42
10	17	271.57	0.71	272.72	1.15	10	17	271.5	272.81	1.31
10	18	275.19	0.65	273.41	-1.78	10	18	275.3	273.50	-1.80

Table A.9: Y_{res} for **DU11** in Short-Period (RUN 8000-8085). All quantities are represented in degrees.

(a) Using Yaw mean values.

DU	FLOOR	$Y_{\text{data}}(\text{mean})$	$Y_{\text{data}}(\text{SD})$	$Y_{\text{parameterized}}$	Y_{res}
11	1	274.05	0.23	269.82	-4.23
11	2	274.00	0.26	269.89	-4.11
11	3	267.33	0.32	269.96	2.62
11	4	268.79	0.28	270.02	1.23
11	5	270.44	0.30	270.09	-0.35
11	6	267.40	0.30	270.15	2.75
11	7	266.66	0.32	270.22	3.56
11	8	268.08	0.33	270.29	2.21
11	9	269.47	0.36	270.35	0.89
11	10	273.37	0.38	270.42	-2.95
11	11	268.49	0.39	270.48	1.99
11	12	272.57	0.42	270.55	-2.02
11	13	271.50	0.43	270.62	-0.88
11	14	269.25	0.44	270.68	1.43
11	15	269.30	0.78	270.75	1.45
11	16	271.04	0.47	270.82	-0.22
11	17	270.88	0.46	270.88	0.01
11	18	274.32	0.53	270.95	-3.37

(b) Using Nominal Yaw values.

DU	FLOOR	$Y_{\text{data}}(\text{mode})$	$Y_{\text{parameterized}}$	Y_{res}
11	1	274.0	269.79	-4.21
11	2	273.9	269.85	-4.05
11	3	267.3	269.91	2.61
11	4	268.7	269.97	1.27
11	5	270.4	270.03	-0.37
11	6	267.4	270.09	2.69
11	7	266.6	270.15	3.55
11	8	268.0	270.21	2.21
11	9	269.4	270.26	0.86
11	10	273.3	270.32	-2.98
11	11	268.4	270.38	1.98
11	12	272.5	270.44	-2.06
11	13	271.4	270.50	-0.90
11	14	269.2	270.56	1.36
11	15	268.9	270.62	1.72
11	16	270.9	270.68	-0.22
11	17	270.8	270.74	-0.06
11	18	274.2	270.80	-3.40

Bibliography

- [1] S Adrián-Martínez, M Ageron, F Aharonian, S Aiello, A Albert, F Ameli, E Anassontzis, M Andre, G Androulakis, M Anghinolfi, and et al. Letter of intent for KM3NeT 2.0. *Journal of Physics G: Nuclear and Particle Physics*, 43(8):084001, Jun 2016.
- [2] P Coyle, KM3NeT Collaboration, et al. KM3NeT-ORCA: oscillation research with cosmics in the abyss. In *Journal of Physics: Conference Series*, volume 888, page 012024. IOP Publishing, 2017.
- [3] European Strategy Group Collaboration et al. Update of the european strategy for particle physics. *CERN Council, Geneva*, 2020.
- [4] H Aihara, A Aranda, R Toro, M Cambiaso, M Carena, E Carrera, J d’Olivo, A Gago, T Goncalves, G Herrera, H Yepes, et al. Latin American HECAP Physics Briefing Book. *arXiv preprint arXiv:2104.06852*, 2021.
- [5] S Viola. KM3NeT acoustic positioning and detection system. In *EPJ Web of Conferences*, volume 216, page 02006. EDP Sciences, 2019.
- [6] V Kulikovskiy, G Riccobene, and E Poma. KM3NeT CALIB 2016 0011 PRO AHRS Calibration and Qualification v1. 2016.
- [7] P Piattelli, E Poma, G Riccobene, and Viola S. KM3NeT CALIB 2017 0042PRO AHRS Calibration v5. 2017.
- [8] P Groves. Principles of GNSS, inertial, and multisensor integrated navigation systems, [book review]. *IEEE Aerospace and Electronic Systems Magazine*, 30(2):26–27, 2015.
- [9] J Dow, R Neilan, and C Rizos. The international GNSS service in a changing landscape of global navigation satellite systems. *Journal of geodesy*, 83(3-4):191–198, 2009.
- [10] X Yuan, J Fu, H Sun, and C Toth. The application of GPS precise point positioning technology in aerial triangulation. *ISPRS Journal of Photogrammetry and Remote Sensing*, 64(6):541–550, 2009.
- [11] L Mandrake, B Wilson, C Wang, G Hajj, A Mannucci, and X Pi. A performance evaluation of the operational Jet Propulsion Laboratory/University of Southern California global assimilation ionospheric model (JPL/USC GAIM). *Journal of Geophysical Research: Space Physics*, 110(A12), 2005.

- [12] J McDowell. The low earth orbit satellite population and impacts of the SpaceX Starlink constellation. *The Astrophysical Journal Letters*, 892(2):L36, 2020.
- [13] T Butash, P Garland, and B Evans. Non-geostationary satellite orbit communications satellite constellations history, 2021.
- [14] V Sokolovic, G Dikic, and R Stancic. Integration of ins, gps, magnetometer and barometer for improving accuracy navigation of the vehicle. *Defence Science Journal*, 63(5):451–455, 2013.
- [15] R Allmendinger, C Siron, and C Scott. Structural data collection with mobile devices: Accuracy, redundancy, and best practices. *Journal of Structural Geology*, 102:98–112, 2017.
- [16] H Alkhaldi. Integration of a star tracker and inertial sensors using an attitude update. 2014.
- [17] R Christ and R Wernli. *The ROV manual: a user guide for remotely operated vehicles*. Butterworth-Heinemann, 2013.
- [18] A Alcocer, P Oliveira, and A Pascoal. Underwater acoustic positioning systems based on buoys with GPS. In *Proceedings of the Eighth European Conference on Underwater Acoustics*, volume 8, pages 1–8, 2006.
- [19] C Lv, B Shen, C Tian, S Zhang, L Yu, and D Xu. Signal Design and Processing for Underwater Acoustic Positioning and Communication Integrated System. In *2020 IEEE 3rd International Conference on Information Communication and Signal Processing (ICICSP)*, pages 89–93. IEEE, 2020.
- [20] D Skerritt, C Fitzsimmons, and N Polunin. Fine scale acoustic telemetry as an offshore monitoring and research tool recommended practice. *Marine Biology, Ecosystems and Governance Research Group, NERC*, 2015.
- [21] M Ageron, JA Aguilar, Imen Al Samarai, A Albert, F Ameli, M André, M Anghinolfi, G Anton, S Anvar, M Ardid, et al. ANTARES: the first undersea neutrino telescope. *Nuclear Instruments and Methods in Physics Research Section A: Accelerators, Spectrometers, Detectors and Associated Equipment*, 656(1):11–38, 2011.
- [22] M Ardid. Positioning system of the ANTARES neutrino telescope. *Nuclear Instruments and Methods in Physics Research Section A: Accelerators, Spectrometers, Detectors and Associated Equipment*, 602(1):174–176, 2009.
- [23] AD Avrorin, AV Avrorin, VM Aynutdinov, R Bannash, IA Belolaptikov, VB Brudanin, NM Budnev, AA Doroshenko, GV Domogatsky, R Dvornický, et al. Baikal-GVD: status and prospects. In *EPJ Web of Conferences*, volume 191, page 01006. EDP Sciences, 2018.
- [24] M Agostini, M Böhmer, J Bosma, K Clark, M Danninger, C Fruck, R Gernhäuser, A Gärtner, D Grant, F Henningsen, et al. The Pacific Ocean Neutrino Experiment. *Nature Astronomy*, 4(10):913–915, 2020.
- [25] The Positioning system for KM3NeT, author=Riccobene, G, booktitle=EPJ Web of Conferences, volume=207, pages=07005, year=2019, organization=EDP Sciences.

- [26] CD Llorens, M Ardid, T Sogorb, M Bou-Cabo, J Martínez-Mora, G Larosa, and S Adrián-Martínez. The sound emission board of the KM3NeT acoustic positioning system. *Journal of Instrumentation*, 7(01):C01001, 2012.
- [27] F Caruso, G Alonge, G Bellia, E De Domenico, R Grammauta, G Larosa, S Mazzola, G Riccobene, G Pavan, E Papale, et al. Long-term monitoring of dolphin biosonar activity in deep pelagic waters of the mediterranean sea. *Scientific Reports*, 7(1):1–12, 2017.
- [28] P Gorham, D Saltzberg, P Schoessow, W Gai, R Konecny, and ME Conde. Radio-frequency measurements of coherent transition and cherenkov radiation: Implications for high-energy neutrino detection. *Physical Review E*, 62(6):8590, 2000.
- [29] M Caruso. Applications of magnetic sensors for low cost compass systems. In *IEEE 2000. Position location and navigation symposium (Cat. No. 00CH37062)*, pages 177–184. IEEE, 2000.
- [30] X Zhu, Ta Zhao, D Cheng, and Z Zhou. A three-step calibration method for tri-axial field sensors in a 3d magnetic digital compass. *Measurement Science and Technology*, 28(5):055106, 2017.
- [31] M Ang and V Tourassis. Singularities of euler and roll-pitch-yaw representations. *IEEE Transactions on Aerospace and Electronic Systems*, (3):317–324, 1987.
- [32] R Bruijn and D van Eijk. The KM3NeT multi-PMT DIGITAL optical module. In *The 34th International Cosmic Ray Conference*, volume 236, page 1157. SISSA Medialab, 2016.
- [33] P Musico. The central logic board for the optical module of the KM3NeT detector. In *Technology and Instrumentation in Particle Physics 2014*, volume 213, page 372. SISSA Medialab, 2015.
- [34] D Calvo and D Real. Status of the Central logic Board (CLB) of the KM3NeT neutrino telescope. *Journal of Instrumentation*, 10(12):C12027, 2015.
- [35] P Musico. The Central Logic Board for the optical module of the KM3NeT detector. 2014.
- [36] S Biagi, M Cresta, C Hugon, V Kulikovskiy, P Musico, A Orzelli, A Orlando, and F Pratolongo. AHRS for CLBv2 documentation. 2014.
- [37] STMicroelectronics. LIS3LV02DL, MEMS inertial sensor 3-axis - $\pm 2g/\pm 6g$ digital output low voltage linear accelerometer. 2008.
- [38] Honeywell. 3-Axis Digital Compass HMC5843. 2009.
- [39] STMicroelectronics. LSM303DLHC, Ultra-compact high-performance ecompass module: 3D accelerometer and 3D magnetometer. 2013.
- [40] Dídac D Tortosa. Mechanical Line Fit Model to Monitor the Position of KM3NeT Optical Modules from the Acoustic and Compass/Accelerometer sensor system data. In *Multidisciplinary Digital Publishing Institute Proceedings*, volume 42, page 33, 2019.